



Full paper

## Lithium metal electrode protected by stiff and tough self-compacting separator

Zhuoqun Tang<sup>a,b,1</sup>, Sa Li<sup>a,b,1,\*\*</sup>, Yao Li<sup>c</sup>, Hui Xu<sup>a,b</sup>, Yue Yu<sup>a,b</sup>, Yunhui Huang<sup>a,b,\*\*\*</sup>, Ju Li<sup>d,\*</sup>

<sup>a</sup> School of Materials Science and Engineering, Tongji University, Shanghai, 201804, China

<sup>b</sup> Institute of New Energy for Vehicles, Tongji University, Shanghai, 201804, China

<sup>c</sup> State Key Laboratory of Metal Matrix Composites, Shanghai Jiao Tong University, Shanghai, 200240, China

<sup>d</sup> Department of Nuclear Science and Engineering, Department of Materials Science and Engineering, Massachusetts Institute of Technology, Cambridge, MA, 02139, USA



## ARTICLE INFO

## Keywords:

Artificial SEI

Self-consolidating

Modulus

Toughness

Lithium metal anode

## ABSTRACT

Lithium metal anode (LMA) has exceptionally high capacity and low redox potential. However, lack of stable separator/solid electrolyte that can suppress morphological instabilities of LMA has significantly hampered its use. While high-stiffness solid electrolyte is regarded as a solution to suppress LMA sinusoidal wave instability, the poor toughness and failure tolerance often lead to cracking-based mechanical failures. Here, a facile surface spray of initially loose  $\text{Sb}_2\text{O}_3$  powders on Li metal generates a self-compacting separator (SCS) *in situ* of  $5 \pm 2 \mu\text{m}$  thickness. Electrochemical characterization reveals that such SCS layer allows fast ion migration ( $10^{-4} \text{ S cm}^{-1}$ ) and is electronically insulating, causing Li to precipitate underneath stably and uniformly. Moreover, mechanical examination demonstrates that the SCS is stiff ( $>10 \text{ GPa}$  modulus), tough, and possesses flexibility and self-healing ability. Protected by a SCS, LMA can cycle at  $10 \text{ mA cm}^{-2}/10 \text{ mAh cm}^{-2}$  for 260 h without short-circuiting. When the ultrathin Li@SCS foil (total thickness  $20 \mu\text{m}$ ) is paired against  $\text{LiFePO}_4$  cathode with  $<1.2 \times$  excess Li, it demonstrates stable cycling for 60 cycles at an industrial loading of  $3 \text{ mAh cm}^{-2}$  and a rate of 0.5C, tripling the cycle life compared to unprotected Li. The SCS-covered LMA is also nonflammable in fire for 180s in contrast to unprotected Li foil.

## 1. Introduction

Lithium metal anodes (LMAs) are experiencing a renaissance. In view of Li metal's high theoretical capacity per unit mass/volume and low electrochemical potential, LMAs are considered very promising for future high-energy-density rechargeable batteries. However, LMAs are the least safe among Li anode materials, due to morphological instabilities that lead to electrical short-circuiting across the separator and thermal runaways. The same morphological instabilities and highly reactive nature of lithium metal with electrolyte also result in the formation of electronically insulating solid-electrolyte interphase (SEI) debris that causes loss of cyclable Li, electrolyte dry-out and low Coulombic Efficiency (CE) [1]. For LMA to make it in industry, we believe that three levels of performance requirements are needed. Level 1: The lithium metal batteries must not short-circuit, even under

extremely high areal current density (such as  $10 \text{ mA cm}^{-2}$ ) and capacity (such as  $10 \text{ mAh cm}^{-2}$ ) cycling conditions, because short-circuiting is a safety concern. Level 2: Coulombic Efficiency must be sufficiently high. As there is a tradeoff between the cycling energy density and the full-cell Li inventory, it is easy to show that LMA would not be competitive against graphite anode if it starts out more than  $3.5 \times$  excess Li capacity [2]. Good cycle life in a full cell should also be demonstrated under parsimonious Li excess conditions, which is also reflected by a "good CE". Level 3: When the battery package is breached due to external causes (e.g. automobile accidents involving hitting or burning), the LMA must burn more gently in air, compared to say, gasoline fire in gasoline-fueled car crashes. This requires the lithium to have smaller specific surface area, which again points to suppressing morphological instabilities of Li. Only when level-1, 2, 3 are all satisfied can LMA based batteries become truly competitive in the marketplace.

\* Corresponding author.

\*\* Corresponding author. School of Materials Science and Engineering, Tongji University, Shanghai, 201804, China.

\*\*\* Corresponding author. School of Materials Science and Engineering, Tongji University, Shanghai, 201804, China.

E-mail addresses: [lisa@tongji.edu.cn](mailto:lisa@tongji.edu.cn) (S. Li), [huangyh@tongji.edu.cn](mailto:huangyh@tongji.edu.cn) (Y. Huang), [liju@mit.edu](mailto:liju@mit.edu) (J. Li).

<sup>1</sup> These authors contributed equally to this work.

Since  $\text{Li}_{\text{BCC}}$  morphological instability (LMI) is the root cause of many ills, and the separator is in intimate contact with LMA, researchers have come up with various approaches to engineer the separator in order to suppress LMI. A separator serves the following functions: (a) it is electronically insulating, (b) it remains conductive to  $\text{Li}^+$ , (c) it prevents Li dendrites from poking through (level-1 concern), (d) it keeps the  $\sim 50 \mu\text{m}$  thick LMA in a low-porosity state (level-2, 3 concerns). Standard polymer separators like Celgard (Fig. 1b), dense ceramic solid electrolytes (SE, Fig. 1c), and naturally formed solid-electrolyte interphase layer (Fig. 1d) all satisfy (a), (b) requirements. But they usually fail in (c), (d) requirements, with different causes but all mechanics-related. Standard porous polymer separators ( $\sim 10 \mu\text{m}$  thick) has too wide pores ( $10^2 \text{ nm}$ ), that tip-grown Li dendrite can easily plate through [3, 4]. Naturally formed SEI is too thin (10 nm thick), fragile and easily bursts under pressure, forming extruded root-grown Li whiskers that severely degrade the CE [1,3,5,6]. Dense solid electrolyte has attracted a lot of attention. Monroe and Newman [7] showed that when Li is confined by a SE layer that has more than double the elastic stiffness of  $\text{Li}_{\text{BCC}}$ , the sinusoidal profile instabilities rewarded by kinetic advantage in electrodeposition/stripping can be suppressed due to the elastic energy penalty. This criterion, however, does not consider the possibilities of inelastic processes such as shear relaxation in Li metal, or inelastic deformation or fracture in SE layer. Porz et al. [8] showed that a cracking-based attack mode can self-perpetuate in stiff ceramics that the Monroe-Newman criterion has no defense against. The relevant quantity for suppressing dendrites penetration failure due to the cracking singularity mode attack should be the fracture toughness, not the elastic

stiffness of the SE. In addition, these SEs have been mainly synthesized by *ex-situ* methods [9–12], which are expensive and difficult to scale up.

The emphasis on SE's mechanical toughness and stickiness to Li is relatively recent [13,20] and has resulted in a proliferation of studies that use a treated lithium anode under high current density and high capacity (Table S1). Such  $\sim 10 \mu\text{m}$  thick fully dense ceramic cannot tolerate unavoidable undulations in manufacturing or cycling, and will fracture across the  $\sim 10 \text{ cm}$  width required by industrial batteries, as purely inorganic ceramic materials lack fault tolerance. In terms of flaw tolerance, here we also take cues from biology, where organic-inorganic composites are much stiffer and tougher than individual phases [14,15]. The composites often utilize different phases or structural orientations, to generate hard-core layers so as to resist penetration, and have a viscoelastic organic phase allowing for strain redistribution to accommodate the increased deformation, especially for nanoscale particles (whose failure criterion is governed by the theoretical strength rather than by the Griffith criterion [15]). Besides, cycling an areal capacity of  $10 \text{ mAh cm}^{-2}$  means repeated thickening and thinning of lithium layer by at least  $50 \mu\text{m}$  where voids can nucleate between Li and SE, which can cause serious interfacial contact problem. Thus, compared to liquid electrolyte, it is often not *just* the bulk  $\text{Li}^+$  conductivity of SE that matters, but also the *contact quality* between Li and SE represented by the charge-transfer resistance  $R_{\text{CT}}$  [16].

Motivated by the understandings above, we develop a facile and scalable lithium surface treatment using antimony trioxide ( $\text{Sb}_2\text{O}_3$ ) [17]. When  $\text{Sb}_2\text{O}_3$  is sprayed onto Li surface, the following chemical reactions  $6\text{Li} + \text{Sb}_2\text{O}_3 \rightarrow 2\text{Sb} + 3\text{Li}_2\text{O}$  and  $3\text{Li} + \text{Sb} \rightarrow \text{Li}_3\text{Sb}$ , will happen. These

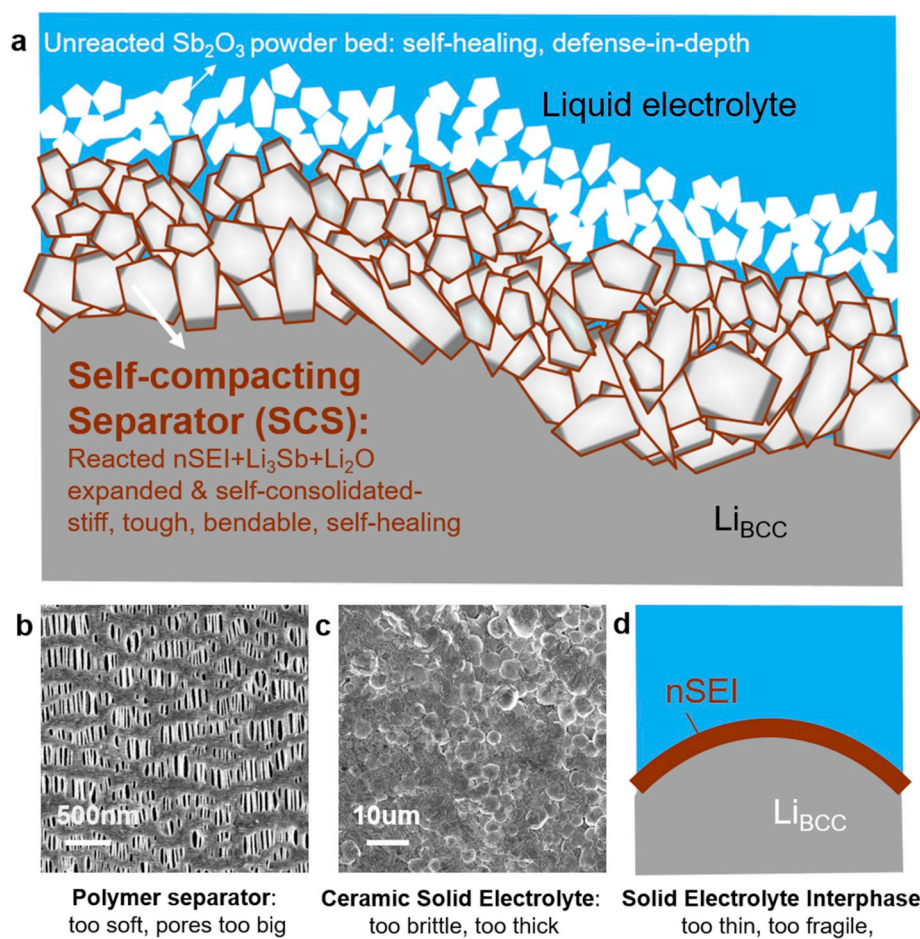


**Fig. 1.** Schematic depicting the function of the SCS-protected lithium foil. **a.** Schematic layout of lithium by SCS film protection, with good stiffness, toughness, adherence, and an excellent room-temperature lithium diffusivity of  $6.8 \times 10^{-4} \text{ S cm}^{-1}$ . **b.** Soft and porous polymer separator. **c.** Dense but fragile ceramic solid electrolyte. **d.** Natural solid electrolyte interface with 10 nm thick on Li metal.

reactions help to form a nano-composite layer (abbreviated as SOL). The SOL layer is semi-consolidated and will leak liquid electrolyte. By using standard carbonate electrolyte, the natural SEI will form adherently and immediately, covering any exposed Sb/Li<sub>3</sub>Sb/Li metal surfaces. The eventual product formed is the self-compacting separator (SCS), with the organic-inorganic composition Sb/Li<sub>3</sub>Sb/Li metal/Li<sub>2</sub>O/nSEI (Fig. 1a), and shown to have with a good stiffness (>10 GPa, guarding against the Monroe-Newman instability which requires at least double the modulus of Li<sub>BCC</sub>, which is 3.4 GPa [7]), toughness (against Porz et al. instability [8]), adherence (guaranteeing low  $R_{CT}$  [16]), and an excellent room-temperature Li<sup>+</sup> diffusivity of  $6.8 \times 10^{-4} \text{ S cm}^{-1}$ . The conversion of SOL→SCS takes place in the first ten cycles or so of electrochemical cycling of the LMA battery, analogous to the “formation” stage of traditional lithium ion batteries (LIBs). We will show that this SCS layer,  $5 \pm 2 \mu\text{m}$  thick, (a): delivers a cycling life of 260 h at an extremely high current density of  $10 \text{ mA cm}^{-2}$  and high capacity of  $10 \text{ mAh cm}^{-2}$  without internal short circuiting and with a polarization of 0.2 V, (b) when paired against commercial LiFePO<sub>4</sub> cathode, with  $1.15 \times$  excess capacity Li<sub>BCC</sub>, the full cell sustains more than 60 cycles at a rate of 0.5C ( $1.3 \text{ mA cm}^{-2}$ ), in contrast to only 20 cycles in unprotected LMA, (c) protected LMA delays air fire for as long as 180 s, a possibly crucial time for people to escape from auto crashes. These indicate that further interphase composite engineering [18–25] with stiff, tough and adherent properties on Li metal electrode could be the next leap needed to solve the Level-1, 2, 3 problems outlined at the start.

## 2. Results and discussion

### 2.1. The conversion of Sb<sub>2</sub>O<sub>3</sub> powders→SOL→SCS *in situ*

As illustrated in Fig. 2a, a controlled amount of Sb<sub>2</sub>O<sub>3</sub> micropowders is sprayed onto Li surface with initial thickness  $d_{\text{spray}}(\text{Sb}_2\text{O}_3)$ , followed by repeated roller pressing. Fig. 2b shows the outcomes of the fresh Li and treated Li. Note that Li is a soft metal, with elastic modulus of  $G(\text{Li}_{\text{BCC}}) = 3.4 \text{ GPa}$ , much smaller than  $G(\text{Sb}_2\text{O}_3) = 20 \text{ GPa}$ . Li has a bulk melting temperature  $T_M = 453.7 \text{ K}$ , so at room temperature,  $T/T_M = 2/3$ , and Li can deform easily by power-law or diffusional creep mechanisms under pressure of the roller. Thus we expect the Li substrate to deform locally and allow some Sb<sub>2</sub>O<sub>3</sub> particles on the bottom to partially sink into it upon pressing by the roller. The surface of Li may be passivated by Li<sub>2</sub>O or Li<sub>2</sub>CO<sub>3</sub>, but they are thin and soft, with shear modulus  $G(\text{Li}_2\text{O}) = 4.5 \text{ GPa}$  [26], and  $G(\text{Li}_2\text{CO}_3) = 21 \text{ GPa}$ , and will surely break with the large mechanical deformation, thus the particles on the bottom will be in direct contact with naked Li. Optically, SOL appears to be black after rolling (before rolling: the sprayed-on Sb<sub>2</sub>O<sub>3</sub> powder bed is silver-gray on lithium substrate).

These reactions cause 240% volume change locally,  $\text{Sb}_2\text{O}_3 (90.38 \text{ \AA}^3) \rightarrow 2\text{Li}_3\text{Sb} (141.264 \text{ \AA}^3) + 3\text{Li}_2\text{O} (75.84 \text{ \AA}^3)$ , as the illustration in Fig. 2c, the product particles on the bottom are bigger and much more densely packed, thus the namesake “self-compacting”. These are also highly exothermic reactions, with 14.9 eV heat released per Sb<sub>2</sub>O<sub>3</sub> decomposed, or  $2.6373 \times 10^{10} \text{ J/m}^3(\text{Sb}_2\text{O}_3)$  and  $4.92 \text{ MJ/kg}(\text{Sb}_2\text{O}_3)$ .

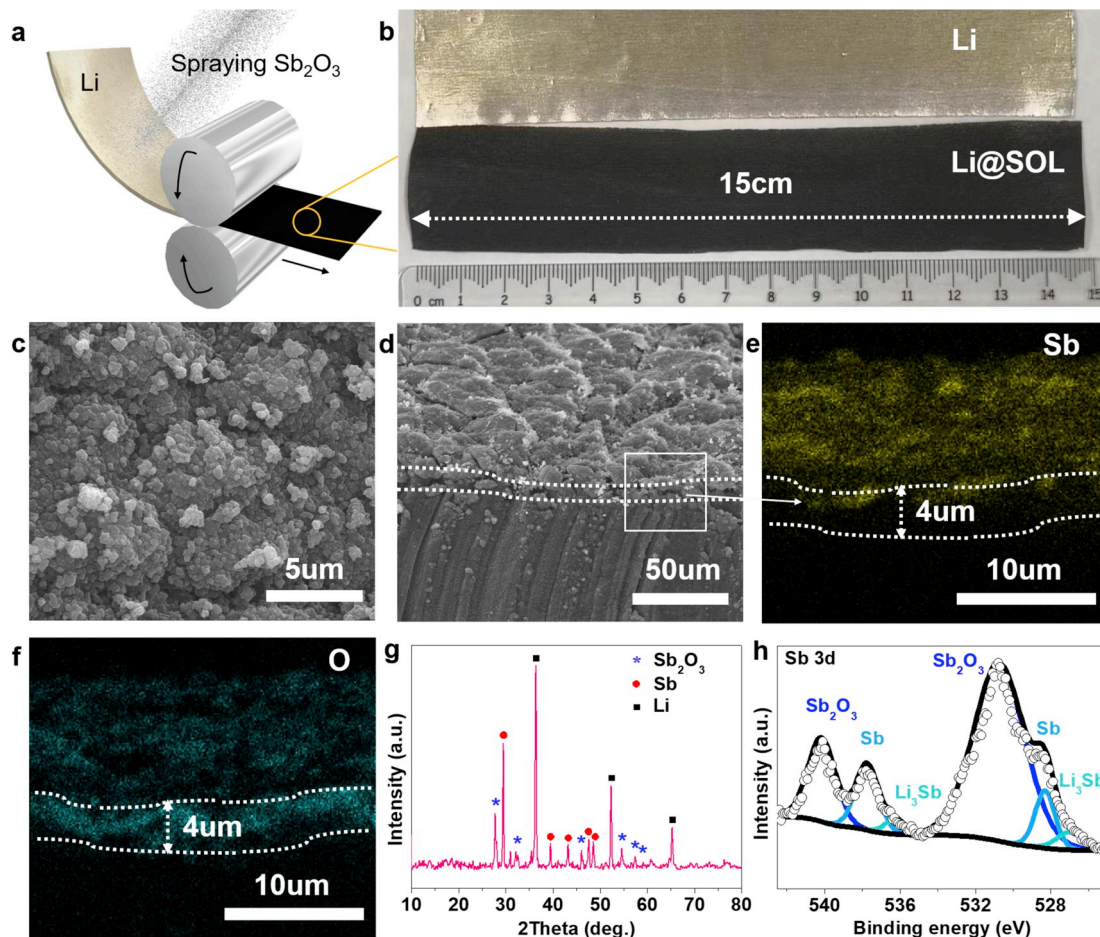


**Fig. 2. Characterization of SOL-protected lithium foil.** a. Schematic illustration of spraying Sb<sub>2</sub>O<sub>3</sub> powder to form a nano passivation layer *in situ*. b. Photo of unprotecting lithium metal compares to the SOL-protected lithium. c. Scanning electron microscopy (SEM) graph of the SOL-protected lithium surface. d. Cross-sectional SEM image of SOL-protected layer. e, f. EDS mapping of Sb and O, respectively, of the cross-section of Li@SOL after spraying Sb<sub>2</sub>O<sub>3</sub> powder. g. X-ray diffraction patterns of SOL-protected lithium metal. h. XPS analysis of SOL-protected lithium metal (before cycling).



For comparison, the gravimetric energy density of TNT explosive is just 4.184 MJ/kg(TNT), and  $\text{Sb}_2\text{O}_3$  has  $3 \times$  the mass density of TNT. Such concentrated volumetric heat release will thus further soften the lithium, and even melt lithium temporarily. So we envision some molten Li metal will reactively wet the  $\text{Sb}_2\text{O}_3$  surfaces and wick up, converting more  $\text{Sb}_2\text{O}_3$  powders into  $\text{Sb}/\text{Li}_3\text{Sb}/\text{Li}_2\text{O}$  (Fig. 2g and 2h). The inorganic  $\text{Sb}/\text{Li}_3\text{Sb}/\text{Li}$  metal/ $\text{Li}_2\text{O}$  (and perhaps  $\text{LiOH}$ ,  $\text{Li}_2\text{CO}_3$  which we define as inorganic) products will form a nano-composite SOL layer with  $d_{\text{SOL}} = 5 \pm 2 \mu\text{m}$  in thickness after compression and sticking tightly to lithium substrate (Fig. 2d).

The SOL layer is semi-consolidated, in the sense that it is not air-tight or liquid-tight like the dense ceramic SE (e.g. Fig. 1c), and will leak liquid electrolyte (Fig. S1), albeit more slowly at the bottom due to the more expanded and compacted nature. There is also unreacted  $\text{Sb}_2\text{O}_3$  in the core of some particles owing to Li exhaustion or heat exhaustion, and there can also be some completely unreacted  $\text{Sb}_2\text{O}_3$  remaining on the top as well, depending on the  $\text{Sb}_2\text{O}_3$  amount we spray on. Energy dispersive spectroscopy (EDS) mapping of the SOL protected Li shows a uniform distribution of Sb and O in the layer (Fig. 2e and 2f). We believe the exothermic reaction  $\rightarrow$  Li melting  $\rightarrow$  reactive wetting  $\rightarrow$  wicking up of Li metal and more exothermic reaction ... process will terminate once the powder bed is thicker than  $\sim 10 \mu\text{m}$ , when there are unreacted powders on top even after pressing, that remain loose in optical microscopy observations once spraying too much (Fig. S2). Such unreacted  $\text{Sb}_2\text{O}_3$  powders "reserve" can cope with large-scale morphological undulation (like Fig. 1a) by granular flow (unlike dense ceramic solid electrolyte which will surely fracture or lose electrical contact or both), and will provide "defense-in-depth" against future lithium dendrites penetration.

The last step is to convert the semi-consolidated, inorganic, SOL layer to consolidated organic-inorganic SCS layer with lower porosity and much enhanced mechanical properties, by wetting the SOL layer with liquid electrolyte and performing electrochemical cycling. The process is quite similar to the setting of concrete, where addition of a liquid and subsequent reactions allow the cementitious binder to glue the aggregate solids and impart the composites with rather exceptional stiffness and toughness [27]. As Fig. S3 shows, with a typical commercial electrolyte 1 M  $\text{LiPF}_6$  in 1:1 EC:DEC with 10%FEC+1%VC, the SOL surface treatment greatly improves the wetting angle of the lithium surface to this electrolyte, from  $21.25^\circ$  to  $7.76^\circ$ . FEC and VC facilitate the formation of a uniform, compact layer with an elastic SEI and high Li-ion conductivity, favorable for the formation of SCS film [28]. Since the SOL is still electrically conductive and is connected to the lithium metal beneath, the electrochemical potential is 0 V everywhere there is electronic percolation to a naked metallic surface exposed to the electrolyte. The carbonate electrolyte will decompose below 0.6 V versus  $\text{Li}^+/\text{Li}$ , thus SEI will form on all naked metallic surfaces immediately [29] and cover up any exposed  $\text{Sb}/\text{Li}_3\text{Sb}/\text{Li}$  metal surfaces in the  $\text{Sb}/\text{Li}_3\text{Sb}/\text{Li}$  metal/ $\text{Li}_2\text{O}$  ( $\text{LiOH}/\text{Li}_2\text{CO}_3$ ) nanocomposites. The final SCS should have the composition SEI/ $\text{Sb}/\text{Li}_3\text{Sb}/\text{Li}$  metal/ $\text{Li}_2\text{O}$ . It may still be porous, but with decreasing permeability toward the Li metal side. The electronic conductivity is expected to decrease.

## 2.2. Suppressing the dendrites by SCS protection

The *in situ* formation of SOL $\rightarrow$ SCS is aided by carbonate-based electrolytes. In the first few cycles and in some areas, different formation rates contribute to fluctuant voltages, but everything becomes stabilized in less than 10 cycles, similar to the formation stage of commercial LIBs.

The electrodeposition/stripping of lithium at an ultra-high capacity and current density ( $10 \text{ mAh cm}^{-2}$  at  $10 \text{ mA cm}^{-2}$ ) in symmetrical cells verifies the remarkable effect of SCS layer on LMA stability. With unprotected lithium anode, SEI thickening causes gradual increase in voltage polarization; then electrical short circuiting occurs at 50 h due to growth of dendrites, corresponding to the sharp drop in voltage polarization. In contrast, the SCS-protected lithium shows a very stable

voltage profile over a long period of time up to 260 h (Fig. 3a). In addition, we carefully compare the plating and stripping voltage curves under different areal current density and capacity (Fig. S4). From Fig. S4a, with prolonged cycling, it exhibits a depressed nucleation peak that makes the curve more square-wave-like, indicating a decreasing  $\text{Li}_{\text{BCC}}$  metal nucleation barrier. Very initially, before lithium plating, SEI layer is tightly adhered to Li substrate (right after electrolyte is injected, before electrochemical cycling, the SEI is already formed). When lithium plating initiates,  $\text{Li}^+$  needs to pass through SEI to meet the electrons from underlying Li metal and get reduced at the interface between SEI and Li substrate. Therefore, the freshly deposited lithium metal has to separate the SEI from the substrate to make room for the newly deposited atoms, causing the nucleation polarization. One can imagine nucleating against the pressure exerted by the stretched SEI, that may break and expand the SEI also. As the cycling continues, during stripping, the expanded SEI can sag back a little but not fully goes back, because some void would be left in-between [1,3], which leads to smaller nucleation barrier in later depositions. Note that the similar situation also occurs under lower current density and capacity, such as  $5 \text{ mA cm}^{-2}/5 \text{ mAh cm}^{-2}$  and  $3 \text{ mA cm}^{-2}/3 \text{ mAh cm}^{-2}$  (Figs. S4b and S4c). At the industrially more likely condition of  $3 \text{ mAh cm}^{-2}$  and  $1 \text{ mA cm}^{-2}$ , the SCS-protected Li foil could cycle for more than 1,000 h without any sign of short circuiting (Fig. S5a), while unprotected Li foil suffers from short circuits due to dendrites within 220 h (Fig. S5b).

The postmortem morphology of Li was examined by scanning electron microscopy (SEM). After electrochemical cycling ( $10 \text{ mAh cm}^{-2}$  at  $10 \text{ mA cm}^{-2}$ ) for 20 cycles, the surface of unprotected Li foil showed many cracks ranging from 5 to  $20 \mu\text{m}$  in opening width, and many bulky pores with different depths (Fig. 3b and 3c). Such openings could result from both local preferential dissolution and stress-induced fracture. Upon reversing the current, this could generate more dendritic electrodeposition sites compared with the planar surface due to the concentrated lithium ion flux. Liquid electrolyte penetrates deeply into the cracks, resulting in more consumption of salt, solvent and active lithium. In contrast, the surface of SCS-protected Li was covered by densely compacted nanoparticles, which resembled pavements with a myriad of hard stones showing high structural consistency during cycling (before cycling: Fig. 2c and 2d and after cycling: Fig. 3d and 3e) [30]. The  $\text{Li}_{\text{BCC}}$  foil protected by SCS ( $\text{Li}@\text{SCS}$ ) can be cycled deeply at high current density and capacity on account of a generally uniform lithium ion flux without local hotspots and no significant cracks or delamination [31].

To observe the volume variations of unprotected Li and  $\text{Li}@\text{SCS}$  electrodes during cycling, the morphological changes were investigated by an optically transparent cell (Supporting Information Note 1) to visualize the *operando* (de)lithiation process (Videos S1 and S2). Another Li foils were used as the counter-electrodes without any separator, and an alternating current ( $10 \text{ mA cm}^{-2}$  for 360s plating and stripping) was applied. Fig. 3h and 3i showed the photos taken at different cycles.

Supplementary video related to this article can be found at <https://doi.org/10.1016/j.nanoen.2019.104399>

We could see that before cycling, the surfaces of both electrodes were smooth. At 780s, however, clusters of Li deposits began to grow in unprotected Li, resulting in needle-like, tree-like and bush-like LMIs that aggregated on the top to form high-surface-area  $\text{Li}_{\text{BCC}}$ . In the following stripping cycle, the deposited Li shrunk and its color became darker and darker. However, it did not fully shrink back, which indicates that the reaction with electrolyte and the development of porosity [32,33] result in electronically disconnected and dead Li. Using 3D full-focus optical imaging that scans the focal depth to map out the tomographic surface, we could see that unprotected Li foil became uneven granular Li with obvious filaments and voids after just 5 cycles (Fig. 3f). The increased electrode surface area aggravated detrimental electrolyte decomposition, forming highly porous and bloated structures with total thickness up to  $674 \mu\text{m}$  thicker than the original foil. These are the root causes of poor cycle life when LMA is used in limited Li inventory full-cells.

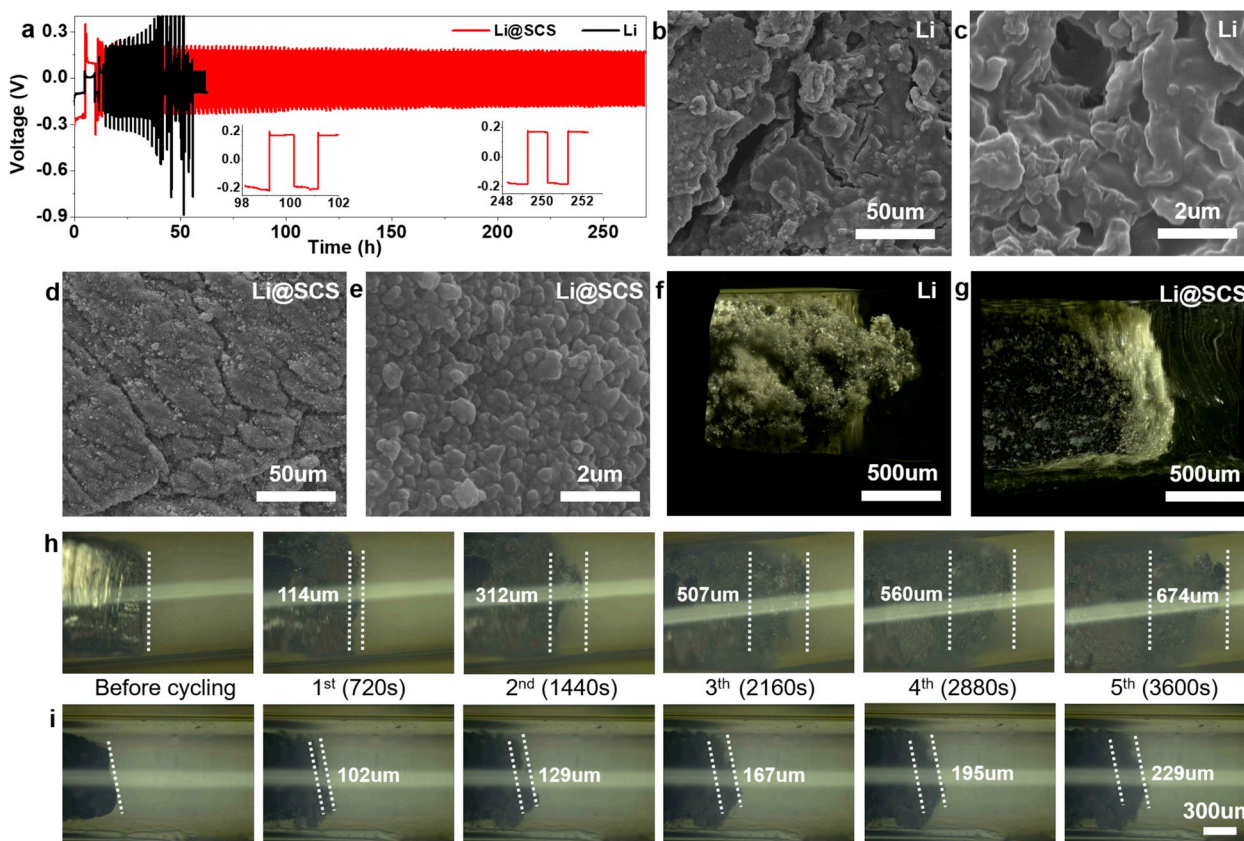


**Fig. 3.** Li metal plating/stripping from symmetric cells and SEM/optical micrograph of the unprotected Li and Li@SCS foils in 1M LiPF<sub>6</sub> 1:1=EC: DEC (10% FEC + 1%VC) electrolyte. **a.** Voltage profile of unprotected Li and Li@SCS anode at 10 mA cm<sup>-2</sup> for 10 mAh cm<sup>-2</sup>, showing the stability at specific times. **b,c,d,e.** SEM images of the surfaces of two electrodes: (b,c) unprotected Li and (d,e) Li@SCS foils in symmetric cells after 20 cycles at 10 mA cm<sup>-2</sup> for 10 mAh cm<sup>-2</sup>. **f,g.** With a through-focus scanning optical microscope, 3D fitting images of (f) unprotected Li and (g) Li@SCS after 5 cycles at 10 mA cm<sup>-2</sup> for 1 mAh cm<sup>-2</sup>. **h,i.** Operando optical microscopy images of the front surfaces of two electrodes, (h) unprotected Li and (i) Li@SCS in a symmetric transparent cell, recorded at 10 mA cm<sup>-2</sup> current density during specified times of plating/stripping. The scale bar in h,i is the same, as indicated.

In contrast, the SCS-protected Li exhibited smooth deposition with no sign of penetrating dendrites or fractal morphology. The electrodeposition/stripping of Li had a quite flat and dense surface with closely packed individual grains of Li metal, and achieved a parallel shift to the initial profile (Fig. 3g). The thickness increased by at most 229 μm, when no external stack pressure was applied. Note that during the first few cycles, the conversion of SOL to SCS (similar to the formation stage of commercial LIBs) has not completed, and therefore large volume change is observed. As the SCS gradually stabilized, the Li@SCS foil volume expanded much less than unprotected Li<sub>BCC</sub>, as shown in Fig. S6. The presence of Li<sub>3</sub>Sb nanoparticles and the buffering function of the Li<sub>2</sub>O matrix help to relieve volume changes and stabilize the structure [34,

35]. Thanks to the constraint of the stiff, tough and adherent SCS layer with nanoscopic pores at the bottom, there was no easy access for micro Li dendrites to grow through.

### 2.3. SCS layer with excellent electronic impedance, stiffness and toughness

#### 2.3.1. High electronic impedance

Due to the large band gap of many SOL components, including Li<sub>2</sub>O (4.9eV), Sb<sub>2</sub>O<sub>3</sub> (3.3eV) and Li<sub>3</sub>Sb (0.7eV), the electronic conductivity is low but might still not be a perfect electronic insulator. We have carried out a measurement of the vertical electronic resistance, which shows

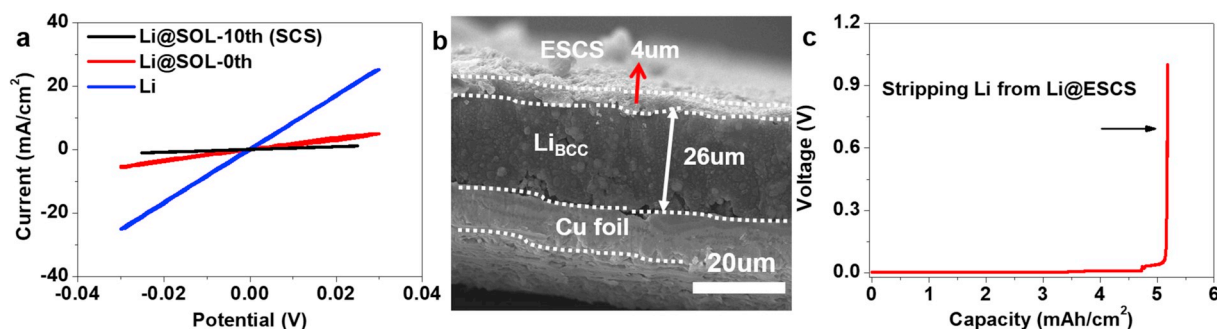


**Fig. 4.** Lithium deposition under the SOL and SCS layer. **a.** The cell polarization curves of Li, Li@SOL and Li@SCS electrodes recorded with 5 mV s<sup>-1</sup> scan rate, which are sandwiched between two stainless steel electrodes. **b.** Cross-sectional SEM image of composite film plated with Li at 0.3 mA cm<sup>-2</sup> for 20 h on Cu foil. **c.** Voltage versus capacity curve of pulling out the Li from Fig. 4b protected foil.

that the SOL layer has electronic conductivity  $0.606 \times 10^4 \Omega \text{ cm}$  initially (Fig. 4a). With further cycling in battery cells, combined with the insertion of SEI, the SCS layer further shuts down electron transportation. The electronic resistivity of the layer after 10 cycles rises to  $4.497 \times 10^4 \Omega \text{ cm}$ . Both  $0.606 \times 10^4 \Omega \text{ cm}$  and  $4.497 \times 10^4 \Omega \text{ cm}$  are much higher than the critical  $13 \Omega \text{ cm}$  needed to induce Li plating beneath a layer that sits atop the current collector (Supporting Information Note 2) [21,36].

To further validate the above claim that  $\text{Li}_{\text{BCC}}$  is deposited beneath SOL/SCS layer, we have also prepared the protection layer in another slightly different way. We first mix 95% $\text{Sb}_2\text{O}_3$ +5%PVDF slurry in NMP solvent, and then directly coat this slurry ( $\sim 5 \mu\text{m}$ ) on bare Cu current collector. We then electroplate Li to this  $\text{Cu@Sb}_2\text{O}_3$  electrode directly with a voltage below 0 V (Fig. S7). Since the  $\text{Sb}_2\text{O}_3$  comes into contact with Li electrochemically, we define the product film produced this way “electrochemical self-compacting separator” (ESCS). ESCS and SCS have very similar properties. The plated Li (totally  $6 \text{ mAh cm}^{-2}$ ) can be divided into two parts. The thickness of the reversibly deposited Li - about  $26 \mu\text{m}$  - is in agreement with that expected for the quantity of Li that can be stripped away ( $5.182 \text{ mAh cm}^{-2}$ ), as shown in Fig. 4c. From the cross-sectional SEM graph (Fig. 4b), we find that Li is assuredly deposited *beneath* this ESCS layer. The other irreversible Li consumption by  $\text{Sb}_2\text{O}_3$  can be calculated by the discrepancy between deposited Li and stripped Li ( $6 - 5.182 = 0.818 \text{ mAh cm}^{-2}$ ). This ESCS protection layer is compositionally invariant in subsequent cycling (Fig. S8 XPS), which

once again affirms its electronically insulating nature.

What’s more, the typical charge profile in a half-cell with  $\sim 100 \times$  excess lithium and *without any commercial separator* against commercial  $\text{LiFePO}_4$  as shown in Fig. S9. This curve proves the SCS layer can shut down electron transportation totally since the cell without any polymer separator has a normal open voltage and a charge plateau. This SCS layer may not be fully solidified and dense sometimes because it was originally in the form of powder, so there can be cracking in some locations. So it is recommended to add commercial separators in practical use.

### 2.3.2. Good stiffness and toughness

The mechanical characteristics of SCS layer are key for suppressing LMIs: suppressing the Monroe-Newman type [7] LMI by high stiffness, and suppressing the Porz et al. [8] type LMI by toughness.

The stiffness of the SCS layer was evaluated by using depth-dependent nanoindentations to compare unprotected Li and  $\text{Li@SCS}$  foil (Fig. 5a). The apparent modulus of  $\text{Li@SCS}$  foil decreases from 11.04 to 0.75 GPa within 0–500 nm and remains unchanged afterwards. The apparent modulus of the unprotected Li foil ranges from 6.15 to 0.16 GPa, and is significantly lower than those of  $\text{Li@SCS}$ , proving the enhanced mechanical stiffness with the addition and compaction of the hard particles [37]. We note that while the SCS layer is  $5 \mu\text{m}$  thick, indenting several hundred nanometers into it would likely trigger inelastic response of the SCS as well as the  $\text{Li}_{\text{BCC}}$  beneath. Thus, only the first tens of nanometers indentation depth gives the true elastic response

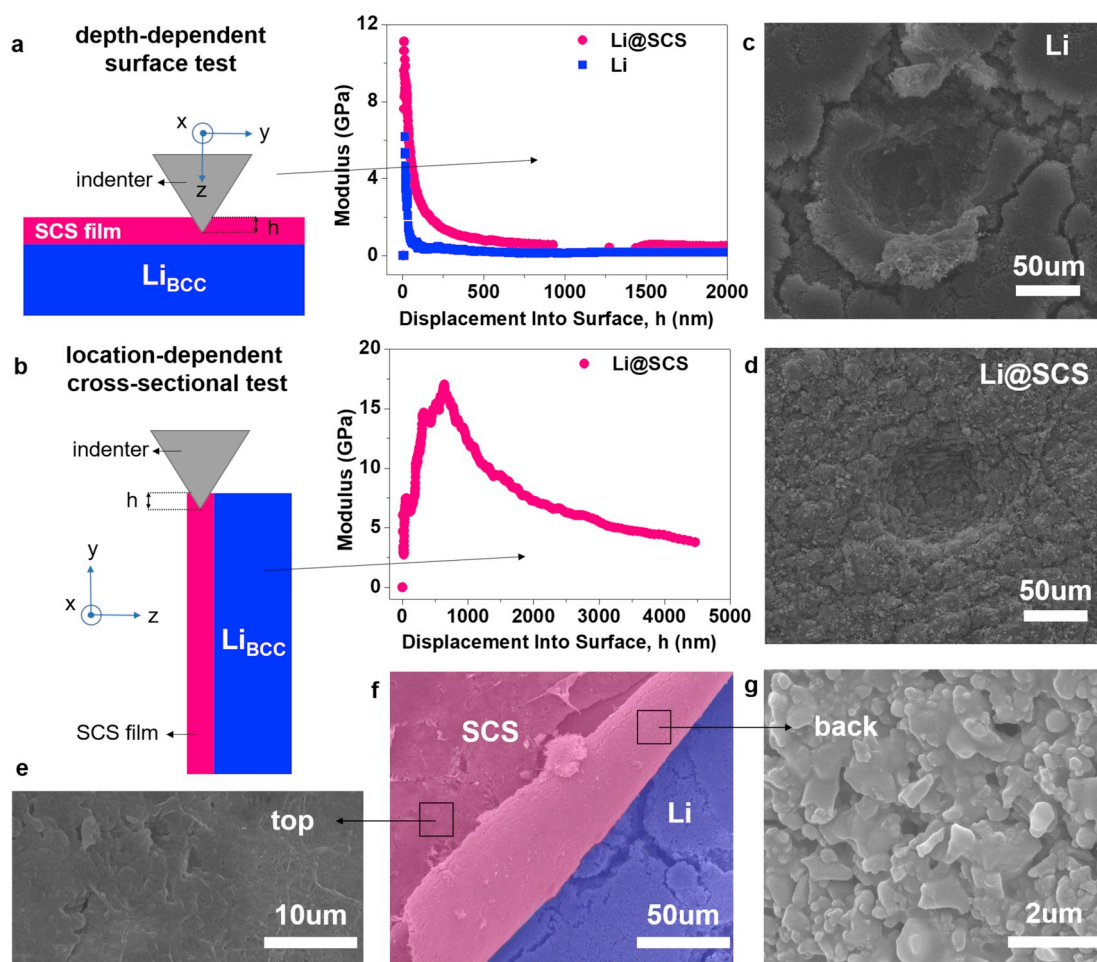


**Fig. 5.** The performance of SCS to restrain Li metal morphological instabilities. **a.** Apparent modulus versus depth curves of the top-view surface of Li and  $\text{Li@SCS}$  foil after 1 cycle at  $10 \text{ mA cm}^{-2}$  for 1 h between the indenter and the nSEI/SCS. **b.** Apparent modulus of the cross-sectional of  $\text{Li@SCS}$  foil. **c,d.** Indentation damage in the surface views of (c) unprotected Li and (d)  $\text{Li@SCS}$  after 10 cycles at  $10 \text{ mA cm}^{-2}$ . **e, f, g.** SEM image of the  $\text{Li@SCS}$  foil at  $10 \text{ mA cm}^{-2}$  after 150 h in a symmetric cell (f) with false color, illustrating the well-compacting layer structure. The upper SCS layer (red region) can effectively safeguard the bottom lithium (blue region). (e) The surface and (g) the back of SCS zooming in from the black marking on Fig. 5f.



of the 5  $\mu\text{m}$  thick SCS film, so 11.04 GPa is certainly above  $2 \times$  the elastic modulus of  $\text{Li}_{\text{BCC}}$  (3.4 GPa). To avoid the plastic response of the soft Li metal base beneath, we can also perform location-dependent cross-sectional indentation tests (Fig. 5b). The SCS layer shows a remarkable apparent modulus exceeding 17 GPa and an average modulus exceeding 10 GPa ranging from 200 nm to 1300 nm, again proving that the SCS possesses sufficient stiffness for suppressing Monroe-Newman sinusoidal-wave LMI [7].

In contrast to Monroe-Newman type sinusoidal-wave instability which requires high elastic stiffness, protecting against Porz et al. [8] type cracking attack requires high degree of toughness and flexibility of the SCS layer. We developed a needle damage experiment that is simple to implement, where the needle probe poked at the electrolyte-facing surface of Li and Li@SCS foil after cycling aggressively at 10 mAh  $\text{cm}^{-2}$  and 10 mA  $\text{cm}^{-2}$  for ten cycles, trying to break or delaminate it from the substrate (Fig. 5c and 5d). Surface ring cracks form in both of them, but unprotected Li shows larger scale of cracks far deeper and wider than that of Li@SCS. This is attributed to the nano-scale composite structure of SCS which ensures good strength, adhesion as well as tolerance of flaws. The composite structure, composed of hard and soft phases (referred to inorganics and organics, respectively), causes the crack to continually change direction, retarding crack growth via the extrinsic toughening mechanism of crack deflection [38].

Then, to again check the toughness of the SCS layer, we have mechanically bent and poked at Li@SCS foil [39]. After mechanically peeling it off from Li (Fig. 5f), the SCS layer (red region) on top of Li metal foil (blue region) can be rolled up. The SCS is seen to be so flexible that it can curl by an angle of  $>400^\circ$  across a radius of curvature of  $\sim 10 \mu\text{m}$ , something that a monolithic ceramic SE certainly cannot do without gross fracture. But before the SOL $\rightarrow$ SCS formation, the SOL layer consisting of inorganic particles alone does not have such good mechanical flexibility yet, as it can fracture like the loose sand piles when we bend the Li foil (Fig. S10). This proves that the electrolyte decomposition products that glue inorganic particles together impart the whole film with good mechanical flexibility and toughness, like the protein-ceramic hybrid structure in bones and nacre with high tenacity. Fig. 5g presents an enlargement of Fig. 5f, showing that the back of SCS-protected lithium is covered by densely packed micro- and nano-sized particles [40]. Li dendrites are suppressed under this rigid and tortuous particulates compact (Fig. 5e).

The percolating pore size at the bottom of the SCS is seen to be very narrow and it is thermodynamically disadvantageous for micro Li dendrites to plate through such small pores, reducing the possibility of short-circuiting [4], while still allowing for facile  $\text{Li}^+$  diffusion through the nanoscale pore channels [41]. Additionally, the residual  $\text{Sb}_2\text{O}_3$  inside compacted particles on the bottom and the unreacted  $\text{Sb}_2\text{O}_3$  on top of the SCS that can still undergo granular flow gives the SCS layer self-healing ability, as any dendrites trying to break through will be consumed by chemical reactions, and actuate new organic-inorganic composite particles to expand and close the pores or microcracks.

#### 2.4. Keeping the $\sim 50 \mu\text{m}$ thick LMA in a low-porosity state

Although Li dendrites can be suppressed well at high current density with the help of stiff and tough SCS layer, cycling at an industrial capacity means repeated thickening and thinning of  $\text{Li}_{\text{BCC}}$  where voids between Li and SE can cause serious contact problems. Also, the total amount of SEI can still grow uncontrollably, leading to high impedance and capacity fading. To check this, electrochemical impedance spectra (EIS) tests were measured during cycling, which exhibit an interesting contrast for the charge-transfer resistance, that signifies the growth in nominal SEI thickness or void/gas pore layers that prevent  $\text{Li}^+$ (electrolyte) +  $e^+$ (metallic) =  $\text{Li}_{\text{BCC}}$  from happening. This is defined as the "contact quality" between a generic electrolyte and the  $e^+$ (metallic)-conducting  $\text{Li}_{\text{BCC}}$ .

Fig. 6a and 6b show the EIS results of unprotected Li and Li@SCS

after different electrodeposition/stripping cycles in symmetric cells. Initially, the unprotected Li electrode showed a combined resistance of 160  $\Omega$  from the SEI layer ( $R_{\text{SEI}}$ ) and charge-transfer reaction ( $R_{\text{CT}}$ ). After 80 h, the resistance of the combined semicircle became about 60  $\Omega$ . The decrease at initial cycling is typical of an electrochemical surface area that is increased by repeated surface reactions. In Li@SCS electrode, the impedance values ( $R_{\text{SEI}} + R_{\text{CT}}$ ) were 350  $\Omega$  right after cell assembly, but showed a much lower value of 22  $\Omega$  after 80 h owing to better contact. The results clearly indicate that this SCS layer protects Li metal from morphological instabilities and enhances  $\text{Li}^+$  reduction kinetics across the interface (low  $R_{\text{CT}}$ ). The ionic conductivity of the SCS determined from EIS is  $6.8 \times 10^{-4} \text{ S cm}^{-1}$  (Supporting Information Note 3), which is comparable with that of the liquid electrolyte ( $10^{-3} \text{ S cm}^{-1}$ ) [42].

The contact quality between Li and SE can also be represented by the polarization voltage between the charge and discharge plateaus (Fig. 6c). When the  $\text{LiFePO}_4$  (LFP)//Li battery was assembled, the cell with SCS-protected layer initially exhibited a large polarization of 123 mV compared to unprotected Li cell (99 mV) because of the extra layer and the requisite formation process. But after 100 cycles, the SCS layer effectively suppresses the LMIs and the growth of SEI and void/gas pores, and the polarization for Li@SCS cell (207 mV) is lower than that for unprotected Li cell (254 mV), reflecting a more stable contact quality.

To demonstrate that Li@SCS can actually lead to a more competitive LMB [43] in the industrial context, we have constructed full-cell battery against commercial LFP as the cathode. From a full cell-energy calculation [1] we have identified that if the LMA has more than  $3.5 \times$  excess Li (e.g.  $3.5 \times 3 \text{ mAh cm}^{-2}$  worth of  $\text{Li}_{\text{BCC}}$  to start with), then the LMB will no longer be competitive against LIB in volumetric energy density that uses graphite anode. Thus, realistic Li-metal batteries cannot use too thick Li foil.

The thinnest commercially available Li foil in the market is mainly 50  $\mu\text{m}$ , which corresponds to 10 mAh  $\text{cm}^{-2}$ , or  $3.7 \times$  excess Li. For making the low excess full cell, this commercial Li foil is too thick [43]. Trying to thin down such Li foil by mechanical rolling is difficult because Li reacts with  $\text{Cr}_2\text{O}_3$  and sticks to the stainless steel surface, which make peeling off the thinned foil impossible without rupturing the soft Li. Therefore, to make matched full cell the researchers always simply electrodeposited some Li on bare Cu foil (10  $\mu\text{m}$ ), which amounts to at least 30  $\mu\text{m}$  total thickness ( $> 10 \mu\text{m}$  Cu + 15.5  $\mu\text{m}$  ( $3.1 \text{ mAh cm}^{-2}$ ) Li if fully dense), since electroplating resulted in a porous state in our experiments with  $3.1 \text{ mAh cm}^{-2}$  Li. In contrast, the ultra-thin Li@SCS foils can be fabricated by a one-step process. With the  $\text{Sb}_2\text{O}_3$  powders sprayed on, it separates Li from the stainless steel roller and reduces the stickiness, allowing the foil to peel off from the roller after rolling without rupturing the soft Li. This simple one-step process is quite similar to making thin dumpling dough skin by sprinkling extra flour on it to reduce stickiness with the wooden rolling pin. The Li@SCS electrode, thinned down to 20  $\mu\text{m}$  in a fully dense state (4.5  $\mu\text{m}$  SCS layer + 15.5  $\mu\text{m}$  ( $3.1 \text{ mAh cm}^{-2}$ ) Li, Fig. S11), is highly amenable to roll-to-roll manufacturing.

When cycling at the rate of 0.5C in Fig. 6d and Fig. S12, the same mass Li anode ( $3.1 \text{ mAh cm}^{-2}$ ) by Li deposition on Cu foil sustains less than 20 cycles (80% capacity retention), with CE dropping to 96.08% within only 10 cycles. However, the Li@SCS anode with equal weight of Li ( $3.1 \text{ mAh cm}^{-2}$ ), with 33% less thickness and 89% less weight (as it is freestanding without the heavy Cu), can maintain more than 60 cycles with an average CE of 99.39%. The cycling stability of thicker Li and Li@SCS foils (both 100  $\mu\text{m}$  thick) is also compared in the full-cell configuration with  $3 \text{ mAh cm}^{-2}$  LFP, where the SCS-protected Li foil can sustain more than 170 cycles with 92% capacity retention and an average CE of 99.81%, while unprotected Li foil decays rapidly from the 80th cycle on, with chaotic CEs.

Fire safety in breached packages is another critical consideration. So we tested the flammability of the anode (Videos S3 and S4). When the flame approached the surface of unprotected Li, only for 30s, it ignited

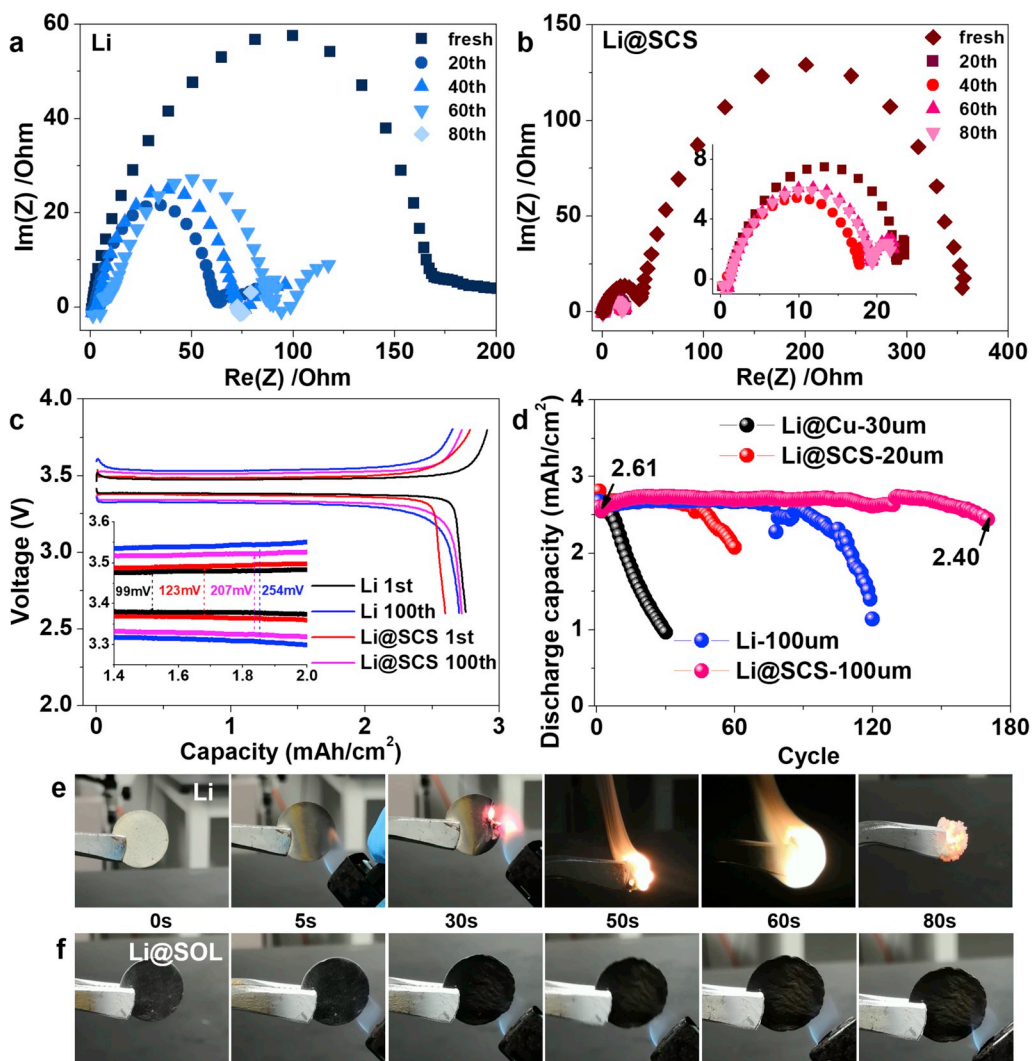


**Fig. 6.** Performance of LiFePO<sub>4</sub>/1.0M LiPF<sub>6</sub> in EC/DEC=1:1 (10%FEC + 1% VC)/Li system in full cells and the safety for protected foil. **a, b.** Electrochemical impedance spectra of (a) unprotected Li (b) Li@SCS electrodes in the symmetric cells after different cycles at 2.5 mA cm<sup>-2</sup>. **c.** The typical charge/discharge profiles in ~3 mAh cm<sup>-2</sup> LFP//~100 μmLi (or Li@SCS) cells. A constant current of 1 mA cm<sup>-2</sup> is applied, corresponding to the rate of 0.36C. **d.** Full-cell results where the Li mole ratio of cathode to anode is set up to 1 (2.7 mAh cm<sup>-2</sup>): 1.15 (3.1 mAh cm<sup>-2</sup>). The initial SOL-protected Li anode (20 μm = 4.5 μm SOL film + 15.5 μm (3.1 mAh cm<sup>-2</sup>) Li) is prepared by spraying powders and rolling foil. The initial unprotected Li anode (1.15 × excess, 3.1 mAh cm<sup>-2</sup>) is prepared by depositing Li on Cu foil at a constant current of 0.05 mA for 62 h. The 100 μm thick Li foil is commercially available and 100 μm thick Li@SCS foil is fabricated by spraying powders and rolling. **e, f.** The reaction of (e) unprotected Li and (f) Li@SOL foils to ignition at different number of seconds.

suddenly and burned violently. In contrast, the SOL protected foil could not be ignited even when it was exposed to the open flame for 180 s (Fig. 6e and 6f). Sb<sub>2</sub>O<sub>3</sub> is actually a commonly used, cheap fire retardant [17], often used in conjunction with halogen-containing compounds [44]. Our result is likely because when Sb<sub>2</sub>O<sub>3</sub> is heated together with halogenated compounds (LiF-rich SEI [5,45], as well as residual fluorinated salts of the liquid electrolyte), the synergistic effect of the mixture creates the flame retardant properties, at least before later cycling when too much dead lithium has formed. This behavior, depending on the electrolyte and number of cycles, will possibly provide crucial time for people to escape from auto crashes.

Supplementary video related to this article can be found at <https://doi.org/10.1016/j.nanoen.2019.104399>

### 3. Conclusions

We have shown that self-compacting nanocomposite separator, generated by a simple surface solid-solid reaction, provides a stable interface for lithium electrodeposition/stripping, to avoid short circuiting caused by dendrites (Level 1), improve cycle life of realistically matched industrial cells (Level 2), and reduce the risk of ignition and explosion even if the cell packaging is breached (Level 3). Furthermore, the unreacted Sb<sub>2</sub>O<sub>3</sub> powders can cope with large-scale morphological undulation of the anode surface by granular flow, and provide “defense-in-depth” against future Li penetration. Specifically, the nanocomposite

SCS is stiff beyond 10 GPa and delivers fast ion conductivity of  $6.8 \times 10^{-4}$  S cm<sup>-1</sup>, which enable suppression of short-circuiting in a symmetric cell over 260 h (10 mA cm<sup>-2</sup> for 10 mAh cm<sup>-2</sup>). It triples the full-cell cycle life under parsimonious Li excess condition, while saving 33% less thickness and 89% less weight, than that of unprotected Li electrodeposited on Cu. Our finding provides a simple and inexpensive strategy to improve the cycling performance and enhance the safety of rechargeable LMBs.

### Declaration of competing interest

There are no conflicts to declare.

### Acknowledgements

The authors are grateful for assistance by Dr. Zhenfeng Qiang in nanoindentations characterization. The authors are also grateful for the support from Tongji University and the National Natural Science Foundation of China (NSFC–No. 51602222, 51632001 and 51972236). JL acknowledges support by Samsung Advanced Institute of Technology.

### Appendix A. Supplementary data

Supplementary data to this article can be found online at <https://doi.org/10.1016/j.nanoen.2019.104399>.

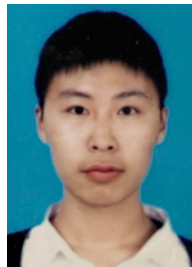


## References

- [1] S. Li, M. Jiang, Y. Xie, H. Xu, J. Jia, J. Li, Developing high-performance lithium metal anode in liquid electrolytes: challenges and progress, *Adv. Mater.* 30 (2018) 1–29, <https://doi.org/10.1002/adma.201706375>.
- [2] Y. Jin, S. Li, A. Kushima, X. Zheng, Y. Sun, J. Xie, J. Sun, W. Xue, G. Zhou, J. Wu, F. Shi, R. Zhang, Z. Zhu, K. So, Y. Cui, J. Li, Self-healing SEI enables full-cell cycling of a silicon-majority anode with a coulombic efficiency exceeding 99.9%, *Energy Environ. Sci.* 10 (2017) 580–592, <https://doi.org/10.1039/c6ee02685k>.
- [3] A. Kushima, K.P. So, C. Su, P. Bai, N. Kuriyama, T. Maebashi, Y. Fujiwara, M. Z. Bazant, J. Li, Liquid cell transmission electron microscopy observation of lithium metal growth and dissolution: root growth, dead lithium and lithium flotsams, *Nano Energy* 32 (2017) 271–279, <https://doi.org/10.1016/j.nanoen.2016.12.001>.
- [4] P. Bai, J. Li, F.R. Brushett, M.Z. Bazant, Transition of lithium growth mechanisms in liquid electrolytes, *Energy Environ. Sci.* 9 (2016) 3221–3229, <https://doi.org/10.1039/c6ee01674j>.
- [5] L. Suo, W. Xue, M. Gobet, S.G. Greenbaum, C. Wang, Y. Chen, W. Yang, Y. Li, J. Li, Fluorine-donating electrolytes enable highly reversible 5-V-class Li metal batteries, *Proc. Natl. Acad. Sci. U.S.A.* 115 (2018) 1156–1161, <https://doi.org/10.1073/pnas.1712895115>.
- [6] F. Wu, Y.X. Yuan, X.B. Cheng, Y. Bai, Y. Li, C. Wu, Q. Zhang, Perspectives for restraining harsh lithium dendrite growth: towards robust lithium metal anodes, *Energy Storage Mater* 15 (2018) 148–170, <https://doi.org/10.1016/j.ensm.2018.03.024>.
- [7] C. Monroe, J. Newman, The impact of elastic deformation on deposition kinetics at lithium/polymer interfaces, *J. Electrochem. Soc.* 152 (2005) 396–404, <https://doi.org/10.1149/1.1850854>.
- [8] L. Porz, T. Swamy, B.W. Sheldon, D. Rettenwander, T. Frömling, H.L. Thaman, S. Berendts, R. Uecker, W.C. Carter, Y.M. Chiang, Mechanism of lithium metal penetration through inorganic solid electrolytes, *Adv. Energy Mater.* 7 (2017) 1–12, <https://doi.org/10.1002/aem.201701003>.
- [9] M. Saccoccio, J. Yu, Z. Lu, S.C.T. Kwok, J. Wang, K.K. Yeung, M.M.F. Yuen, F. Ciucci, Low temperature pulsed laser deposition of garnet Li<sub>6</sub>.4La<sub>3</sub>Zr<sub>1.4</sub>Ta<sub>0.6</sub>O<sub>12</sub> films as all solid-state lithium battery electrolytes, *J. Power Sources* 365 (2017) 43–52, <https://doi.org/10.1016/j.jpowsour.2017.08.020>.
- [10] Z. Huang, W. Pang, P. Liang, Z. Jin, N. Grundish, Y. Li, C.A. Wang, A dopamine modified Li<sub>6</sub>.4La<sub>3</sub>Zr<sub>1.4</sub>Ta<sub>0.6</sub>O<sub>12</sub>/PEO solid-state electrolyte: enhanced thermal and electrochemical properties, *J. Mater. Chem. A* 7 (2019) 16425–16436, <https://doi.org/10.1039/c9ta03395e>.
- [11] A.A. Assegie, J.H. Cheng, L.M. Kuo, W.N. Su, B.J. Hwang, Polyethylene oxide film coating enhances lithium cycling efficiency of an anode-free lithium-metal battery, *Nanoscale* 10 (2018) 6125–6138, <https://doi.org/10.1039/c7nr09058g>.
- [12] K.K. Fu, Y. Gong, B. Liu, Y. Zhu, S. Xu, Y. Yao, W. Luo, C. Wang, S.D. Lacey, J. Dai, Y. Chen, Y. Mo, E. Wachsman, L. Hu, Toward garnet electrolyte-based Li metal batteries: an ultrathin, highly effective, artificial solid-state electrolyte/metallic Li interface, *Sci. Adv.* 3 (2017) 1–12, <https://doi.org/10.1126/sciadv.1601659>.
- [13] D. Devaux, K.J. Harry, D.Y. Parkinson, R. Yuan, D.T. Hallinan, A.A. MacDowell, N. P. Balsara, Failure mode of lithium metal batteries with a block copolymer electrolyte analyzed by X-ray microtomography, *J. Electrochem. Soc.* 162 (2015) A1301–A1309, <https://doi.org/10.1149/2.0721507jes>.
- [14] U.G.K. Wegst, H. Bai, E. Saiz, A.P. Tomsia, R.O. Ritchie, Bioinspired structural materials, *Nat. Mater.* 14 (2015) 23–36, <https://doi.org/10.1038/nmat4089>.
- [15] H. Gao, B. Ji, I.L. Jäger, E. Arzt, P. Fratzl, Materials become insensitive to flaws at nanoscale: lessons from nature, *Proc. Natl. Acad. Sci. U.S.A.* 100 (2003) 5597–5600, <https://doi.org/10.1073/pnas.0631609100>.
- [16] S. Wenzel, D.A. Weber, T. Leichtweiss, M.R. Busche, J. Sann, J. Janek, Interphase formation and degradation of charge transfer kinetics between a lithium metal anode and highly crystalline Li<sub>7</sub>P<sub>3</sub>S<sub>11</sub> solid electrolyte, *Solid State Ion.* 286 (2016) 24–33, <https://doi.org/10.1016/j.ssi.2015.11.034>.
- [17] M. Si, J. Feng, J. Hao, L. Xu, J. Du, Synergistic flame retardant effects and mechanisms of nano-Sb<sub>2</sub>O<sub>3</sub> in combination with aluminum phosphinate in poly(ethylene terephthalate), *Polym. Degrad. Stab.* 100 (2014) 70–78, <https://doi.org/10.1016/j.polymdegradstab.2013.12.023>.
- [18] R. Koerver, W. Zhang, L. De Biasi, S. Schweidler, A.O. Kondrakov, S. Kolling, T. Brezesinski, P. Hartmann, W.G. Zeier, J. Janek, Chemo-mechanical expansion of lithium electrode materials-on the route to mechanically optimized all-solid-state batteries, *Energy Environ. Sci.* 11 (2018) 2142–2158, <https://doi.org/10.1039/c8ee00907d>.
- [19] N.S. Grundish, C.D. Amos, A. Agrawal, H. Khani, J.B. Goodenough, Low-cost self-assembled oxide separator for rechargeable batteries, *Adv. Funct. Mater.* 29 (2019) 1–9, <https://doi.org/10.1002/adfm.201903550>.
- [20] K. Liu, P. Bai, M.Z. Bazant, C.A. Wang, J. Li, A soft non-porous separator and its effectiveness in stabilizing Li metal anodes cycling at 10 mA cm<sup>-2</sup> observed in situ in a capillary cell, *J. Mater. Chem. A* 5 (2017) 4300–4307, <https://doi.org/10.1039/c7ta00069c>.
- [21] X. Liang, Q. Pang, I.R. Kochetkov, M.S. Sempere, H. Huang, X. Sun, L.F. Nazar, A facile surface chemistry route to a stabilized lithium metal anode, *Nat. Energy* 2 (2017) 1–7, <https://doi.org/10.1038/nenergy.2017.119>.
- [22] J. Huang, X. Guo, X. Du, X. Lin, J.Q. Huang, H. Tan, Y. Zhu, B. Zhang, Nanostructures of solid electrolyte interphases and their consequences for micro-sized Sn anodes in sodium ion batteries, *Energy Environ. Sci.* 12 (2019) 1550–1557, <https://doi.org/10.1039/c8ee03632b>.
- [23] C. Yan, X.B. Cheng, Y.X. Yao, X. Shen, B.Q. Li, W.J. Li, R. Zhang, J.Q. Huang, H. Li, Q. Zhang, An armored mixed conductor interphase on a dendrite-free lithium-metal anode, *Adv. Mater.* 30 (2018) 1–9, <https://doi.org/10.1002/adma.201804461>.
- [24] Q. Pang, X. Liang, I.R. Kochetkov, P. Hartmann, L.F. Nazar, Stabilizing lithium plating by a biphasic surface layer formed in situ, *Angew. Chem. Int. Ed.* 57 (2018) 9795–9798, <https://doi.org/10.1002/anie.201805456>.
- [25] R. Xu, Y. Xiao, R. Zhang, X.B. Cheng, C.Z. Zhao, X.Q. Zhang, C. Yan, Q. Zhang, J. Q. Huang, Dual-phase single-ion pathway interfaces for robust lithium metal in working batteries, *Adv. Mater.* 31 (2019) 1–8, <https://doi.org/10.1002/adma.201808392>.
- [26] M.C. Billone, Y.Y. Liu, R.B. Poeppel, J.L. Routbort, K.C. Goretta, D.S. Kupperman, Elastic and creep properties of Li<sub>2</sub>O, *J. Nucl. Mater.* 141–143 (1986) 282–288, [https://doi.org/10.1016/S0022-3115\(86\)80051-4](https://doi.org/10.1016/S0022-3115(86)80051-4).
- [27] W. Liu, N. Liu, J. Sun, P.C. Hsu, Y. Li, H.W. Lee, Y. Cui, Ionic conductivity enhancement of polymer electrolytes with ceramic nanowire fillers, *Nano Lett.* 15 (2015) 2740–2745, <https://doi.org/10.1021/acs.nanolett.5b00600>.
- [28] H. Zhao, X. Yu, J. Li, B. Li, H. Shao, L. Li, Y. Deng, Film-forming electrolyte additives for rechargeable lithium-ion batteries: progress and outlook, *J. Mater. Chem. A* 7 (2019) 8700–8722, <https://doi.org/10.1039/c9ta00126c>.
- [29] H. Xu, S. Li, C. Zhang, X. Chen, W. Liu, Y. Zheng, Y. Xie, Y. Huang, J. Li, Roll-to-roll prelithiation of Sn foil anode suppresses gassing and enables stable full-cell cycling of lithium ion batteries, *Energy Environ. Sci.* 12 (2019) 2991–3000, <https://doi.org/10.1039/c9ee01404g>.
- [30] C. Wang, H. Wu, Z. Chen, M.T. McDowell, Y. Cui, Z. Bao, Self-healing chemistry enables the stable operation of silicon microparticle anodes for high-energy lithium-ion batteries, *Nat. Chem.* 5 (2013) 1042–1048, <https://doi.org/10.1038/nchem.1802>.
- [31] W. Liu, D. Lin, A. Pei, Y. Cui, Stabilizing lithium metal anodes by uniform Li-ion flux distribution in nanochannel confinement, *J. Am. Chem. Soc.* 138 (2016) 15443–15450, <https://doi.org/10.1021/jacs.6b08730>.
- [32] M.J. Zachman, Z. Tu, S. Choudhury, L.A. Archer, L.F. Kourkoutis, Cryo-STEM mapping of solid-liquid interfaces and dendrites in lithium-metal batteries, *Nature* 560 (2018) 345–349, <https://doi.org/10.1038/s41586-018-0397-3>.
- [33] K.N. Wood, E. Kazyak, A.F. Chadwick, K.H. Chen, J.G. Zhang, K. Thornton, N. P. Dasgupta, Dendrites and pits: untangling the complex behavior of lithium metal anodes through operando video microscopy, *ACS Cent. Sci.* 2 (2016) 790–801, <https://doi.org/10.1021/acscentsci.6b00260>.
- [34] Y. Yuan, F. Wu, Y. Bai, Y. Li, G. Chen, Z. Wang, C. Wu, Regulating Li deposition by constructing LiF-rich host for dendrite-free lithium metal anode, *Energy Storage Mater* 16 (2019) 411–418, <https://doi.org/10.1016/j.ensm.2018.06.022>.
- [35] J. He, Y. Wei, T. Zhai, H. Li, Antimony-based materials as promising anodes for rechargeable lithium-ion and sodium-ion batteries, *Mater. Chem. Front.* 2 (2018) 437–455, <https://doi.org/10.1039/c7qm00480j>.
- [36] G. Zheng, S.W. Lee, Z. Liang, H.W. Lee, K. Yan, H. Yao, H. Wang, W. Li, S. Chu, Y. Cui, Interconnected hollow carbon nanospheres for stable lithium metal anodes, *Nat. Nanotechnol.* 9 (2014) 618–623, <https://doi.org/10.1038/nnano.2014.152>.
- [37] Y. Liu, D. Lin, P.Y. Yuen, K. Liu, J. Xie, R.H. Dauskardt, Y. Cui, An artificial solid electrolyte interphase with high Li-ion conductivity, mechanical strength, and flexibility for stable lithium metal anodes, *Adv. Mater.* 29 (2017) 1–8, <https://doi.org/10.1002/adma.201605531>.
- [38] A. Pineau, A. Amine Benzerga, T. Pardoën, Failure of metals III: fracture and fatigue of nanostructured metallic materials, *Acta Mater.* 107 (2016) 508–544, <https://doi.org/10.1016/j.actamat.2015.07.049>.
- [39] G. Xu, A. Kushima, J. Yuan, H. Dou, W. Xue, X. Zhang, X. Yan, J. Li, Ad hoc solid electrolyte on acidized carbon nanotube paper improves cycle life of lithium-sulfur batteries, *Energy Environ. Sci.* 10 (2017) 2544–2551, <https://doi.org/10.1039/c7ee01898c>.
- [40] H. Bryngelsson, J. Eskhult, L. Nyholm, M. Herranen, O. Alm, K. Edström, Electrodeposited Sb and Sb/Sb<sub>2</sub>O<sub>3</sub> nanoparticle coatings as anode materials for Li-ion batteries, *Chem. Mater.* 19 (2007) 1170–1180, <https://doi.org/10.1021/cm0624769>.
- [41] P. Bai, J. Guo, M. Wang, A. Kushima, L. Su, J. Li, F.R. Brushett, M.Z. Bazant, Interactions between lithium growths and nanoporous ceramic separators, *Joule* 2 (2018) 2434–2449, <https://doi.org/10.1016/j.joule.2018.08.018>.
- [42] J. Liang, X. Li, Y. Zhao, L.V. Goncharova, G. Wang, K.R. Adair, C. Wang, R. Li, Y. Zhu, Y. Qian, L. Zhang, R. Yang, S. Lu, X. Sun, In situ Li<sub>3</sub>PS<sub>4</sub> solid-state electrolyte protection layers for superior long-life and high-rate lithium-metal anodes, *Adv. Mater.* 30 (2018) 1–9, <https://doi.org/10.1002/adma.201804684>.
- [43] S. Chen, C. Niu, H. Lee, Q. Li, L. Yu, W. Xu, J.G. Zhang, E.J. Dufek, M. S. Whittingham, S. Meng, J. Xiao, J. Liu, Critical parameters for evaluating coin cells and pouch cells of rechargeable Li-metal batteries, *Joule* 3 (2019) 1094–1105, <https://doi.org/10.1016/j.joule.2019.02.004>.
- [44] H. Wang, H. Wang, Z. Guo, S. Qi, C. Tian, Flame retardant property of Sb<sub>2</sub>O<sub>3</sub>/SnO<sub>2</sub> and their synergism in flexible PVC, *J. Fire Sci.* 24 (2006) 195–210, <https://doi.org/10.1177/0734904106057259>.
- [45] Y. Yuan, F. Wu, G. Chen, Y. Bai, C. Wu, Porous LiF layer fabricated by a facile chemical method toward dendrite-free lithium metal anode, *J. Energy Chem.* 37 (2019) 197–203, <https://doi.org/10.1016/j.jechem.2019.03.014>.



**Zhuoqun Tang** is currently a Master's degree student in School of Materials Science and Engineering at Tongji University. Her research interest is mainly on lithium metal anode materials for high-energy-density lithium batteries.



**Yue Yu** is currently a Master's degree student in School of Materials Science and Engineering at Tongji University. His research is mainly focused on advanced anode materials for Li ion batteries.



**Sa Li** received her Ph.D. degree in Materials Science and Engineering from Tsinghua University in 2015. Afterwards, she joined the School of Materials Science and Engineering at Tongji University as an assistant professor. Her current research interest is mainly on designing advanced anode materials for lithium-ion batteries and Li-S batteries.



**Yunhui Huang** received his Ph.D. from Peking University in 2000. From 2004 to 2007, he worked with Prof. John Goodenough in the University of Texas at Austin. In 2008, he became a Chair Professor of materials science in Huazhong University of Science and Technology. He is now the Director of the Institute of New Energy for Vehicles in Tongji University. His research group works on rechargeable batteries for energy storage and their electrode materials.



**Dr Yao Li** received his PhD in Material Science from the Shanghai Jiao Tong University, China in 2015. He joined as a research associate at Shanghai Jiao Tong University at 2015. He is working on research of bio-inspired material and carbon material, as well as their application on energy storage and environment treatment.



**Ju Li** is BEA Professor of Nuclear Science and Engineering and Professor of Materials Science and Engineering at MIT. His group (<http://Li.mit.edu>) performs computational and experimental research on mechanical properties of materials, and energy storage and conversion. Ju was elected Fellow of the American Physical Society in 2014 and Fellow of the Materials Research Society in 2017.



**Hui Xu** currently is a Ph.D. candidate in Materials Science and Engineering from Tongji University since 2016. Her current research interest is mainly on high-energy-density advanced anode materials for lithium-ion batteries.

## Supporting Information

### Lithium Metal Electrode Protected by Stiff and Tough Self-Compacting Separator

Zhuoqun Tang<sup>1,2†</sup>, Sa Li<sup>1,2†\*</sup>, Yao Li<sup>3</sup>, Hui Xu<sup>1,2</sup>, Yue Yu<sup>1,2</sup>, Yunhui Huang<sup>1,2\*</sup> and Ju Li<sup>4\*</sup>

<sup>1</sup>School of Materials Science and Engineering, Tongji University, Shanghai 201804, China

<sup>2</sup>Institute of New Energy for Vehicles, Tongji University, Shanghai 201804, China

<sup>3</sup>State Key Laboratory of Metal Matrix Composites, Shanghai Jiao Tong University, Shanghai 200240, China

<sup>4</sup>Department of Nuclear Science and Engineering and Department of Materials Science and Engineering, Massachusetts Institute of Technology, Cambridge, MA 02139, USA

<sup>†</sup>These authors contributed equally to this work

\*Corresponding authors

Email address: [lisa@tongji.edu.cn](mailto:lisa@tongji.edu.cn); [huangyh@tongji.edu.cn](mailto:huangyh@tongji.edu.cn); [liju@mit.edu](mailto:liju@mit.edu)



## Methods

### Preparation of the protected lithium anode.

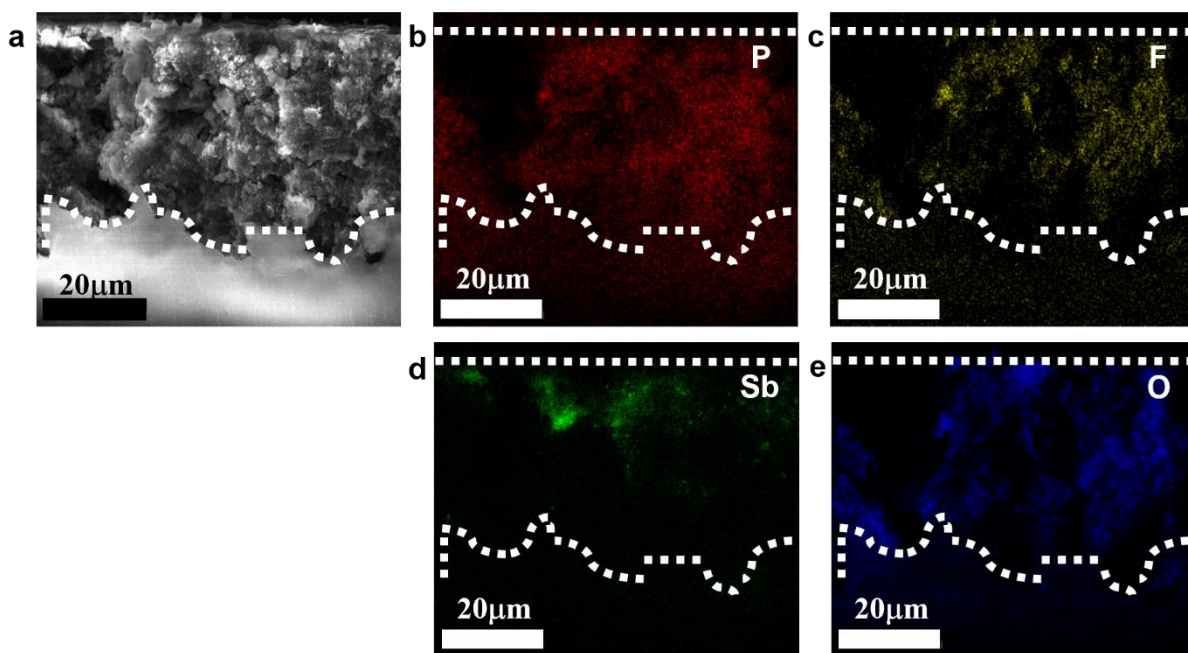
Electrode preparation was carried out in an argon-filled glove box with <1ppm oxygen and moisture. The lithium foil was plastered by antimony trioxide ( $\text{Sb}_2\text{O}_3$ , Alfa, 99.6% min) powders and pressed by roll squeezer. The powders should be spread evenly and excess of them could be blown away with a clean ball, where the amount of  $\text{Sb}_2\text{O}_3$  is about  $5\mu\text{m cm}^{-2}$ . With the addition of carbonate electrolyte, the conversion of  $\text{Li@SOL} \rightarrow \text{Li@SCS}$  takes place in the symmetric cell after a dozen cycles at different current density and capacity (like  $5\text{ mA cm}^{-2}$  for  $5\text{ mAh cm}^{-2}$ ). The  $\text{Li@SCS}$  is exactly what we want. The diameter of the Li metal,  $\text{Li@SOL}$ , and  $\text{Li@SCS}$  anodes are 12mm.

### Materials characterization.

XRD measurements were carried out on a Bruker AXS GMBH GERM D8) with  $\text{CuK}_\alpha$  radiation ( $\lambda = 1.54184\text{ \AA}$ ). The signal was detected for diffraction angles ( $2\theta$ ) between  $10^\circ$  and  $80^\circ$  at a scan rate of  $3^\circ\text{ min}^{-1}$ . The surface and cross-section structure studies were carried out on a field emission scanning electron microscope (SEM, FEI Quanta 200). Discharge–charge cycles of the capillary cells were conducted using the Digital Microscope VHX-2000 instrument with large depth-of-field and 3D imaging. The chamber of an ultrahigh vacuum Imaging XPS Microprobe system for analysis is American Thermo Fisher Scientific ESCALAB 250Xi. The binding energies were calibrated using the C 1s peak at 284.6eV. The modulus of the artificial solid electrolyte film was measured using dynamic displacement nanoindentation (Nano Indenter G200) at a constant strain rate of  $0.2\%\text{ s}^{-1}$ . Poisson's ratio was assumed to be 0.3. All the electrodes were gently washed with DEC to remove the electrolyte salt and dried under vacuum prior to the characterization. The samples were sealed in a vial without exposing the samples to air before being quickly transferred to the system for different analysis.

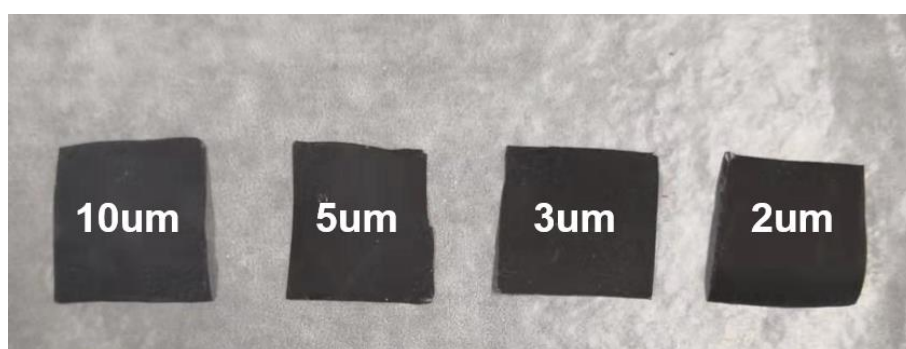
### Electrochemical measurements.

The electrochemical performance was carried out in CR2025 coin-type batteries by Neware test system (CT-4008, Neware). For the lithium plating/stripping studies, symmetric cells (fresh lithium or protected lithium foil on one side) were assembled with  $80\mu\text{l}$  of 1M  $\text{LiPF}_6$  1:1=EC: DEC (10%FEC+1%VC) electrolyte. We used a protocol of 1h of plating followed by 1h of stripping with a current density of  $10\text{ mA cm}^{-2}$ . To investigate the performance of the protection layer compared to the lithium metal anode, full cells were fabricated with  $\text{LiFePO}_4$  as the cathode. The cathodes were cut into disks with a diameter of 12mm. The areal capacity of LFP was about  $2.7\text{ mAh cm}^{-2}$ . The cells were charged-discharged without rest at the desired constant current between 3.8V and 2.6V. Electrochemical impedance measurements were conducted at a VMP-3 with a frequency range of 0.01Hz to 1,000 kHz. All the tests were performed at room temperature.

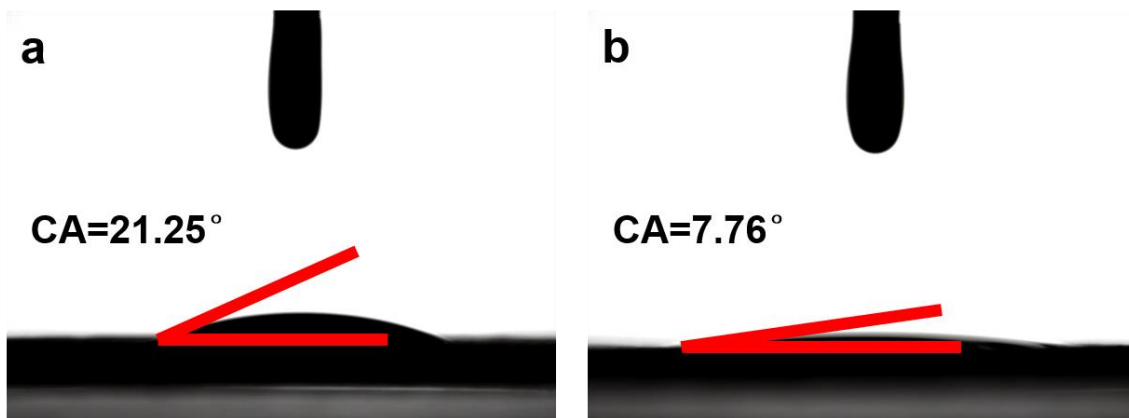


**Figure S1: Cross-sectional SEM images and EDS analysis of SCS-protected lithium anode after  $10 \text{ mA cm}^{-2}$  for 50h. (a)** The cross section of Li@SCS anode, and EDS mapping of (b) phosphorus (c) fluorine (d) antimony (e) oxide corresponding with the cross section image in Fig. S1a.

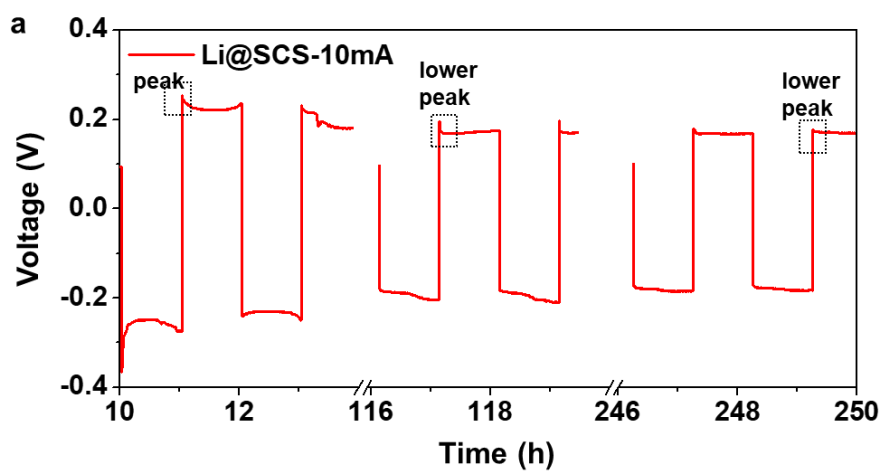
The EDS mapping of P, F, Sb, and O clearly demonstrates the close interfacial contact between the lithium anode and the SCS and the homogeneous distribution of elements in corresponding materials. Sb only distributes in the shallow part of the surface layer, while P and F almost cover the entire cross section, indicating that liquid electrolyte can penetrate through the pores between particles well to form decomposition products which evenly solidify numerous particles of the SOL layer.



**Figure S2:** Different amount of  $\text{Sb}_2\text{O}_3$  powders is sprayed onto Li surface. When  $d_{\text{spray}}(\text{Sb}_2\text{O}_3)$  is superfluous, we could see there are unreacted powders (gray) on top even after pressing.



**Figure S3:** The contact angle of (a) unprotected Li and (b) SOL protected Li. The SOL surface treatment greatly improves the wetting angle of the LMA to the carbonate liquid electrolyte.





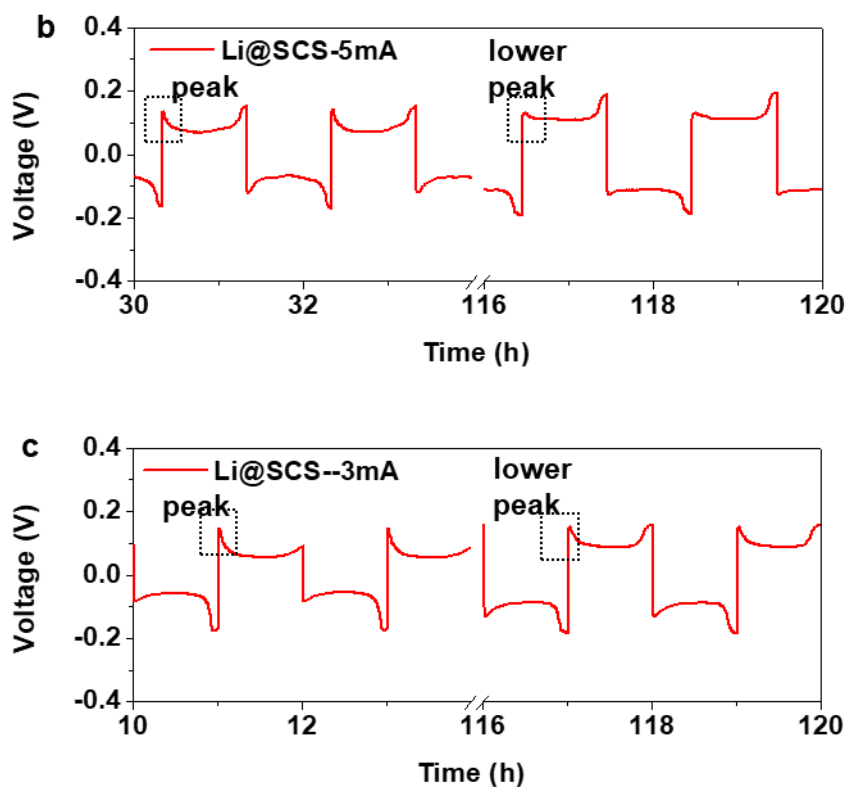


**Figure S4:** Voltage profile of Li@SCS anode at  $10 \text{ mA cm}^{-2}$  for  $10 \text{ mAh cm}^{-2}$ .

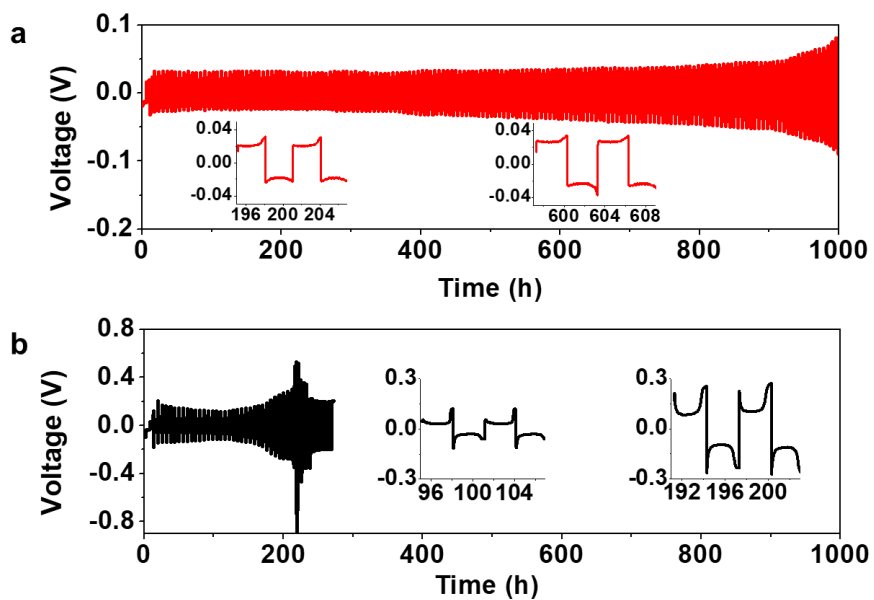


**Figure S5:** Voltage profiles of (a) SCS-protected Li foil and (b) unprotected Li foil at  $1 \text{ mA cm}^{-2}$  and  $3 \text{ mAh cm}^{-2}$ .

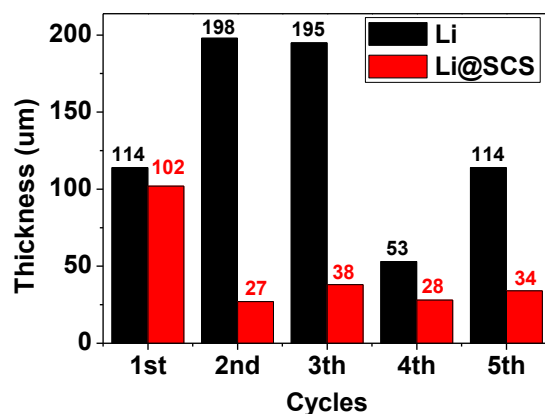


**Figure S6:** The difference value of thickness increase of unprotected Li and Li@SCS during each cycles.

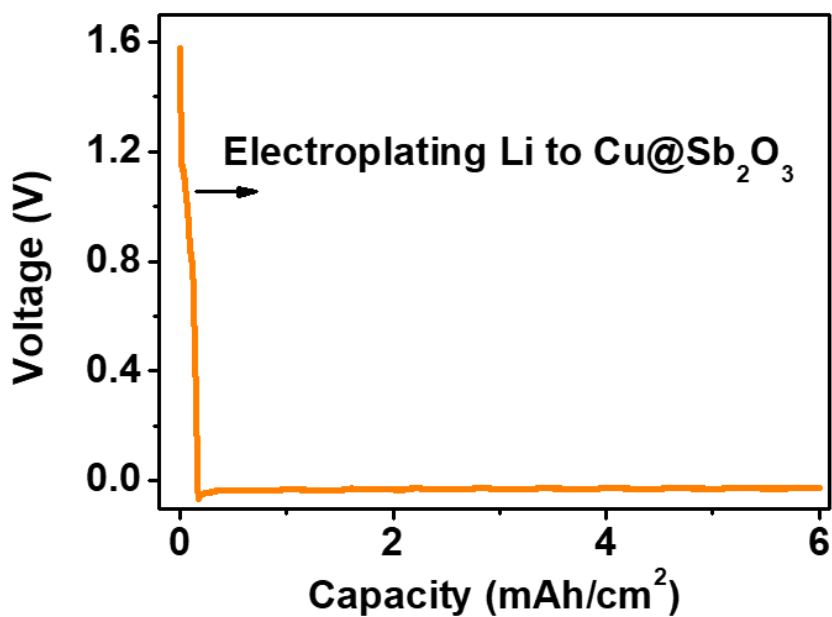


**Figure S7:** Electroplating Li onto Cu@Sb<sub>2</sub>O<sub>3</sub> to form ESCS. We first mix 95%Sb<sub>2</sub>O<sub>3</sub>+5%PVDF slurry in NMP solvent, and then directly coat this slurry on bare Cu current collector. We then electroplate Li at 0.3 mA cm<sup>-2</sup> for 20h onto this electrode until the voltage drops below 0V, illustrating the electronically insulating nature of ESCS.

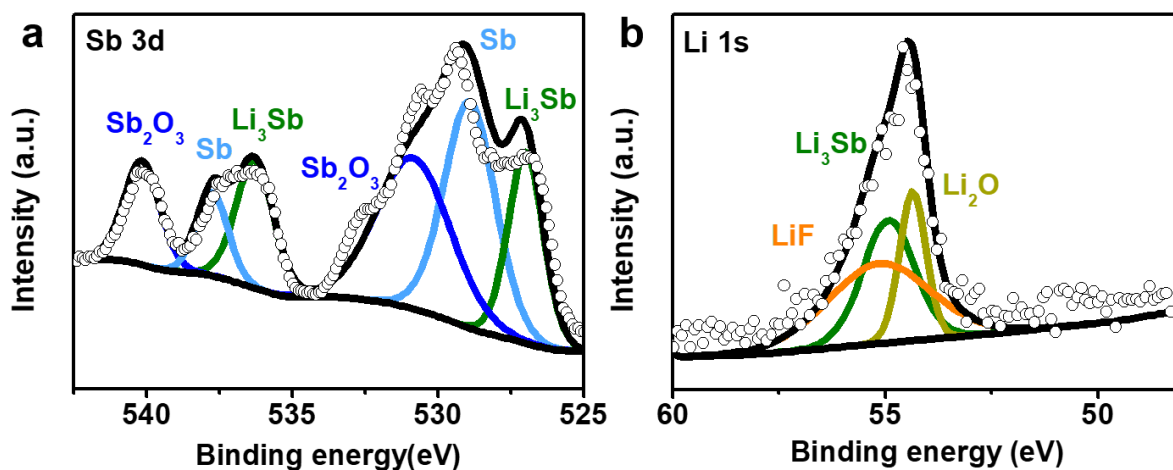


**Figure S8:** XPS analysis of (a) antimony (b) fluorine of the SCS-protected lithium metal after 1 cycle at  $10 \text{ mA cm}^{-2}$  and  $10 \text{ mAh cm}^{-2}$ .

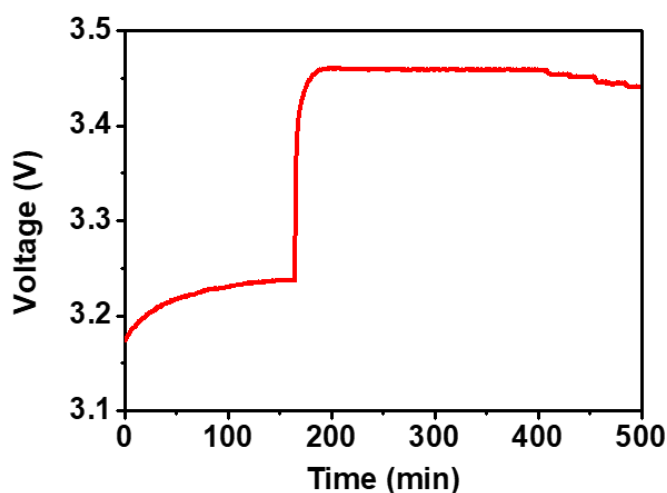


**Figure S9:** The typical charge profile in a half-cell with  $\sim 100\times$  excess lithium and **without any commercial separator** against commercial  $LiFePO_4$ . This curve proves the SCS layer can shut down electron transportation totally since the cell without any commercial polymer separator has a normal open voltage and a charge plateau. The constant current density is  $0.05 \text{ mA cm}^{-2}$ . The conversion of  $Li@SOL \rightarrow Li@SCS$  takes place in the symmetric cell after 10 cycles at  $5 \text{ mA cm}^{-2}$  for  $5 \text{ mAh cm}^{-2}$ . Then the  $Li@SCS$  foil was cut into 16mm disks pairing against 12mm LFP disks.



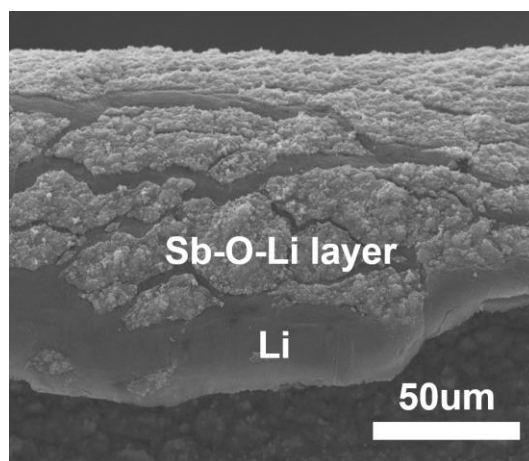


**Figure S10:** SEM image of the protected Li metal foil before cycling (Li@SOL). Coated with  $\text{Sb}_2\text{O}_3$  on both sides of the Li foil, the lithium is soft enough to deform under bending, but the inorganic Sb-O-Li particles cracked and separated from each other.

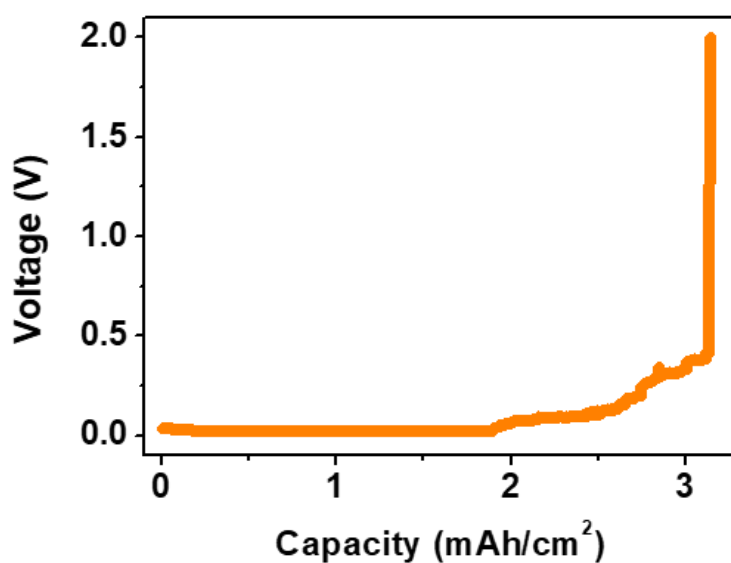


**Figure S11:** Voltage versus capacity profile of delithiation from a  $20\mu\text{m}$  Li@SCS foil that is paired against the pristine Li foil in a cell. The ultra-thin Li@SCS foil is in a fully dense state ( $4.5\mu\text{m}$  SCS film +  $15.5\mu\text{m}$  Li ( $3.1\text{ mAh cm}^{-2}$ )).

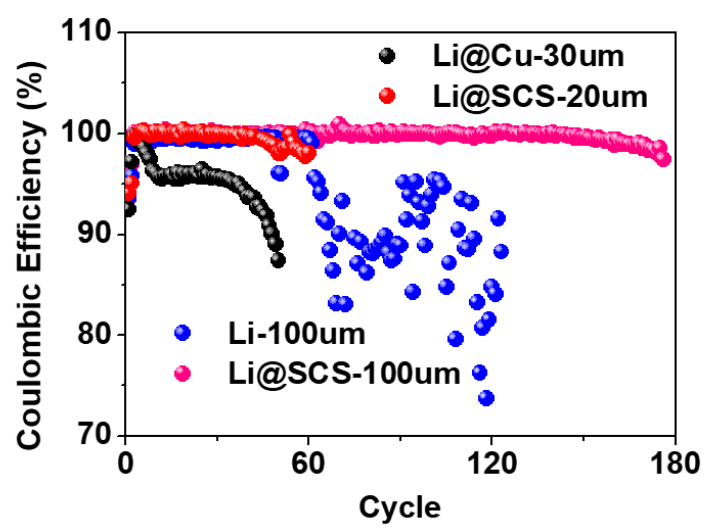


**Figure S12** Coulombic efficiency of Li@Cu-30 $\mu$ m, Li@SCS-20 $\mu$ m, Li-100 $\mu$ m and Li@SCS-100 $\mu$ m in Li | LFP full cell.

**Table S1:** Comparison of the electrochemical performances of the lithium metal anode in symmetric cell between previous reports and our work.

Materials	electrolyte	Current density (mA cm <sup>-2</sup> )	Capacity (mAh cm <sup>-2</sup> )	Cycling performance (h)	References
SCS protection	1M LiPF <sub>6</sub> 1:1=EC:DEC (10%FEC+1% VC)	10	10	260	This work
SCS protection	1M LiPF <sub>6</sub> 1:1=EC:DEC (10%FEC+1% VC)	1	3	1000	This work
elastomeric solid– electrolyte separator	1 M LiPF <sub>6</sub> in EC/EMC	10	10	300	[1]
highly concentrated	4 M LiFSI DME	10	0.5	600	[2]
Li <sub>13</sub> In <sub>3</sub>  Li / LiZn Li	1M LiTFSI 1:1DOL:DME	2	2	1200/1000	[3]
Composite (liquid +polymer) electrolyte	1M LiTFSI DME + PEO + SiO <sub>2</sub>	3	12	800	[4]
3D network gel polymer electrolyte membrane	unknown	2.5	7.5	260	[5]
3D cross-linked network	1.0 M LiTFSI- DOL/DME (1 : 1)	8	8	992	[6]
2D-MoS <sub>2</sub> as a protective layer	1.0 M LiTFSI- DOL/DME (1 : 1)	10	5	300	[7]
LiNO <sub>3</sub> -protected	1M LiPF <sub>6</sub> 1:1=EC:DEC	5	10	290	[8]

### Note 1: Transparent cell fabrication and electrochemical testing

For the LMA symmetric cell without a separator, only one long capillary tube of 1mm diameter was used. A small piece of lithium metal was wrapped around a thin iron wire and was pushed into each end of the capillary, acting as counter and reference electrodes (Figure S13a). After injection of liquid electrolyte, the two open ends of the capillary tubes were sealed and bonded onto a glass slide with epoxy glue (Figure S13b).

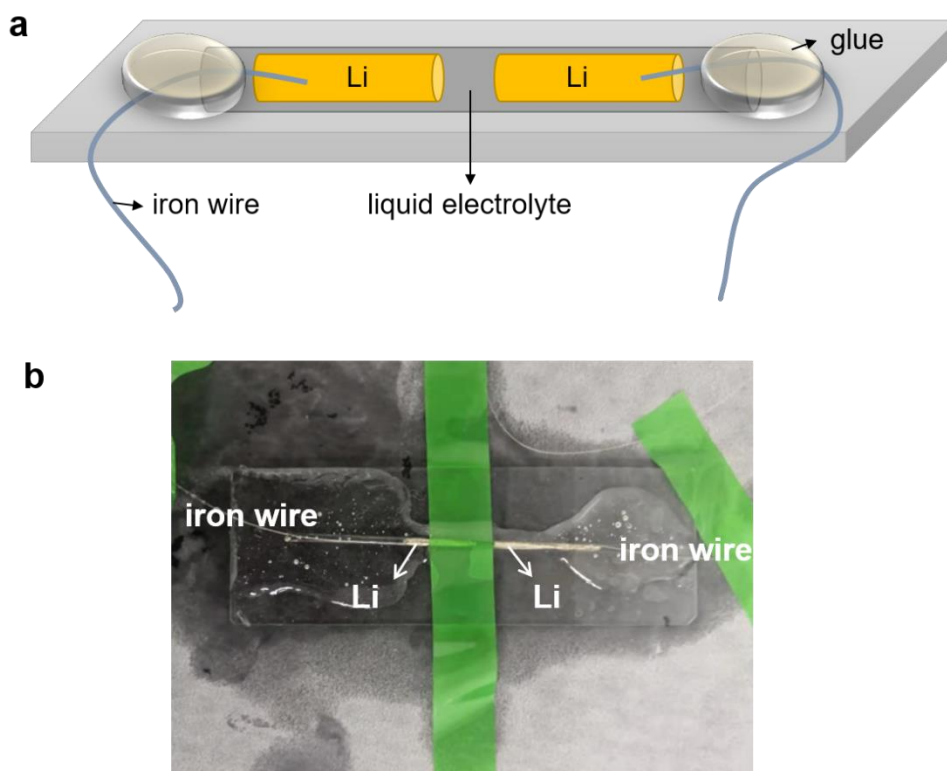


**Figure S13:** (a) Structure of the transparent cell without separator between two electrodes. (b) Photo of the transparent cell.



## Note 2: Electronic resistivity measurement

For resistivity measurement of the SOL→SCS protection film, Li@SOL or Li@SCS foils are sandwiched between two stainless steel electrodes that are Li-blocking but e-receiving (Figure S14). Lithium metal is a good conductor of electrons indicating the expected negligibly small resistivity of lithium metal compared to the protective film [3]. Electronic resistivity ( $\rho$ ) was calculated as following:

$\rho = \frac{U \cdot S}{I \cdot L}$ , where  $L$  is the thickness of the composite protection film;  $I$  is applied current;  $S$  is area of the contact between stainless steel and the foil;  $U$  is average voltage increase.

The total thickness of the protection film is  $2 \times 5 \mu\text{m} = 10 \mu\text{m}$ , namely  $L = 10 \mu\text{m}$ . The calculated values of electronic resistivity for SOL and SCS film is  $6061 \Omega \cdot \text{cm}$  and  $44974 \Omega \cdot \text{cm}$ , respectively. The resistance values are two–three orders of magnitude higher than those of amorphous carbon nanosphere films ( $13 \Omega \cdot \text{cm}$ ) that induce Li plating underneath the film [9].

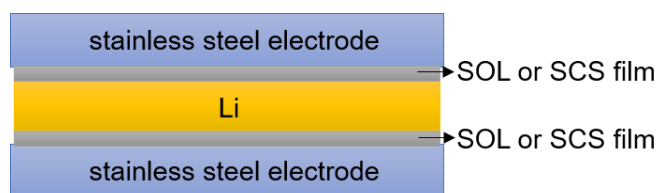


**Figure S14:** Schematic structure of the sandwich cell.

## Supplementary Video

Video S1-*Operando* (de)lithiation process of unprotected Li.

[http://li.mit.edu/S/ZhuoqunTang/Upload/1operando\(de\)lithiation\\_li\\_16xrecordingspeed.mp4](http://li.mit.edu/S/ZhuoqunTang/Upload/1operando(de)lithiation_li_16xrecordingspeed.mp4)

Video S2-*Operando* (de)lithiation process of Li@SCS.

[http://li.mit.edu/S/ZhuoqunTang/Upload/2operando\(de\)lithiation\\_lisb\\_16xrecordingspeed.mp4](http://li.mit.edu/S/ZhuoqunTang/Upload/2operando(de)lithiation_lisb_16xrecordingspeed.mp4)

Video S3- Flammability of unprotected Li.

<http://li.mit.edu/S/ZhuoqunTang/Upload/3flammabilityli.mp4>

Video S4- Flammability of Li@SCS.

<http://li.mit.edu/S/ZhuoqunTang/Upload/4flammabilityli-sb.mp4>

### Note 3: Ionic conductivity measurement

The ionic conductivity ( $\sigma$ ) of the SCS was roughly estimated from EIS measurement in a symmetric cell, according to the equation:  $\sigma=L/RS$ , where  $L$ ,  $R$  and  $S$  are the thickness, the ionic impedance and the contact area of SCS film, respectively. Considering several cycles are usually needed for the formation of SCS film, we select the electrochemical impedance spectra of 20<sup>th</sup> cycle in a symmetric cell for analysis (Figure S15).

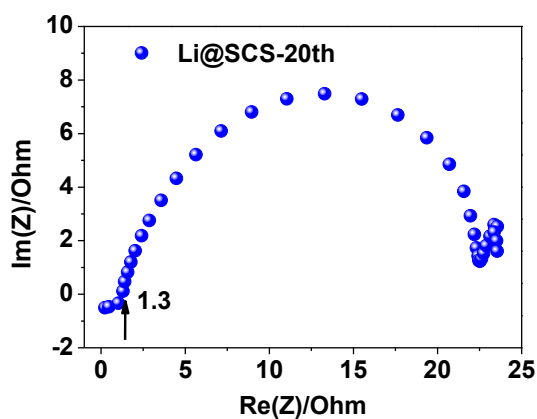


**Figure S15** Electrochemical impedance spectra of Li@SCS electrodes in a symmetric cell after 20 cycles.

The total thickness of the protection film is  $2 \times 5 \mu\text{m} = 10 \mu\text{m}$ , namely  $L = 10 \mu\text{m}$ . The high frequency resistance is the long-range transport resistance, so the value of ionic impedance of SCS is  $1.3 \Omega$ . The diameter of the Li@SCS anode is  $12\text{mm}$  and the value of the area is  $1.13\text{cm}^2$ . The ionic conductivity of the SCS calculated from above is  $6.8 \times 10^{-4} \text{S cm}^{-1}$ .

## References

- [1] K. Liu, P. Bai, M.Z. Bazant, C.A. Wang, J. Li, A soft non-porous separator and its effectiveness in stabilizing Li metal anodes cycling at 10 mA cm<sup>-2</sup> observed in situ in a capillary cell, *J. Mater. Chem. A*. 5 (2017) 4300–4307. <https://doi.org/10.1039/c7ta00069c>.
- [2] J. Qian, W.A. Henderson, W. Xu, P. Bhattacharya, M. Engelhard, O. Borodin, J.G. Zhang, High rate and stable cycling of lithium metal anode, *Nat. Commun.* 6 (2015). <https://doi.org/10.1038/ncomms7362>.
- [3] X. Liang, Q. Pang, I.R. Kochetkov, M.S. Sempere, H. Huang, X. Sun, L.F. Nazar, lithium metal anode, 17119 (2017) 1–7. <https://doi.org/10.1038/nenergy.2017.119>.
- [4] M.S. Park, D.J. Lee, D. Im, S. Doo, O. Yamamoto, A Highly Reversible Lithium Metal Anode, (2014) 1–8. <https://doi.org/10.1038/srep03815>.
- [5] Q. Lu, Y. He, Q. Yu, B. Li, Y.V. Kaneti, Y. Yao, Dendrite-Free , High-Rate , Long-Life Lithium Metal Batteries with a 3D Cross-Linked Network Polymer Electrolyte, (2017). <https://doi.org/10.1002/adma.201604460>.
- [6] K. Deng, D. Han, S. Ren, S. Wang, M. Xiao, Y. Meng, Single-ion conducting artificial solid electrolyte interphase layers for dendrite-free and highly stable lithium metal anodes, *J. Mater. Chem. A*. 7 (2019) 13113–13119. <https://doi.org/10.1039/c9ta02407g>.
- [7] E. Cha, M.D. Patel, J. Park, J. Hwang, V. Prasad, K. Cho, W. Choi, 2D MoS<sub>2</sub> as an efficient protective layer for lithium metal anodes in high-performance Li-S batteries, *Nat. Nanotechnol.* 13 (2018) 337–343. <https://doi.org/10.1038/s41565-018-0061-y>.
- [8] Q. Shi, Y. Zhong, M. Wu, H. Wang, H. Wang, High-capacity rechargeable batteries based on deeply cyclable lithium metal anodes, *Proc. Natl. Acad. Sci. U. S. A.* 115 (2018) 5676–5680. <https://doi.org/10.1073/pnas.1803634115>.
- [9] G. Zheng, S.W. Lee, Z. Liang, H.W. Lee, K. Yan, H. Yao, H. Wang, W. Li, S. Chu, Y. Cui, Interconnected hollow carbon nanospheres for stable lithium metal anodes, *Nat. Nanotechnol.* 9 (2014) 618–623. <https://doi.org/10.1038/nnano.2014.152>.